2007-09

Aging effects on microstructure and creep in Sn-3.8Ag-0.7Cu solder

Cornejo, Orlando A.

Monterey, California. Naval Postgraduate School

NAVAL POSTGRADUATE SCHOOL

MONTEREY, CALIFORNIA

THESIS

AGING EFFECTS ON MICROSTRUCTURE AND CREEP IN Sn-3.8Ag-0.7Cu SOLDER

by

Orlando Cornejo

September 2007

Thesis Advisor: Indranath Dutta

Approved for public release; distribution is unlimited

THIS PAGE INTENTIONALLY LEFT BLANK

REPORT DOCUMENTATION PAGE			Form Approved OMB No. 0704-0188
Public reporting burden for this collection of information is estimated to average 1 hour per response, including the time for reviewing instruction, searching existing data sources, gathering and maintaining the data needed, and completing and reviewing the collection of information. Send comments regarding this burden estimate or any other aspect of this collection of information, including suggestions for reducing this burden, to Washington headquarters Services, Directorate for Information Operations and Reports, 1215 Jefferson Davis Highway, Suite 1204, Arlington, VA 22202-4302, and to the Office of Management and Budget, Paperwork Reduction Project (0704-0188) Washington DC 20503.			
1. AGENCY USE ONLY ***(Leave blank)***	**2. REPORT DATE** September 2007	**3. REPORT TYPE AND DATES COVERED** Master's Thesis	
4. TITLE AND SUBTITLE Aging Effects on Microstructure and Creep in Sn-3.8Ag-0.7Cu Solder		**5. FUNDING NUMBERS**	
6. AUTHOR(S) Orlando Cornejo			
7. PERFORMING ORGANIZATION NAME(S) AND ADDRESS(ES) Naval Postgraduate School Monterey, CA 93943-5000		**8. PERFORMING ORGANIZATION REPORT NUMBER**	
9. SPONSORING /MONITORING AGENCY NAME(S) AND ADDRESS(ES) N/A		**10. SPONSORING/MONITORING AGENCY REPORT NUMBER**	
11. SUPPLEMENTARY NOTES The views expressed in this thesis are those of the author and do not reflect the official policy or position of the Department of Defense or the U.S. Government.			
12a. DISTRIBUTION / AVAILABILITY STATEMENT Approved for public release; distribution is unlimited		**12b. DISTRIBUTION CODE**	

13. ABSTRACT (maximum 200 words)

Solder joints provide mechanical and electrical interconnections between electronic devices and packaging substrates in electronics applications. The different coefficient of thermal expansion (CTE) between substrate, silicon device and solder imposes strains on the solder joint. Creep constitutes the primary deformation mechanism, limiting the low cycle fatigue life of solder joint. The trend toward miniaturization, higher service temperatures, and higher current densities and the transition to lead-free solders, which possess higher melting points than leaded solders, aggravate the situation. Therefore, the knowledge of properties and performances is needed to be able to predict the lifetime of solders in order to assure successfully applications in electronic assemblies. This study focuses on the change of microstructure due aging in bulk and ball joints, and a preliminary analysis of the primary creep behavior of Sn-3.8Ag-0.7Cu. Differences in microstructure evolution between bulk and small joints are highlighted.

14. SUBJECT TERMS Lead-Free, Solders, SAC-387, Microstructure			**15. NUMBER OF PAGES** 95
			16. PRICE CODE
17. SECURITY CLASSIFICATION OF REPORT Unclassified	**18. SECURITY CLASSIFICATION OF THIS PAGE** Unclassified	**19. SECURITY CLASSIFICATION OF ABSTRACT** Unclassified	**20. LIMITATION OF ABSTRACT** UL

NSN 7540-01-280-5500 Standard Form 298 (Rev. 2-89)
Prescribed by ANSI Std. 239-18

THIS PAGE INTENTIONALLY LEFT BLANK

Approved for public release; distribution is unlimited

AGING EFFECTS ON MICROSTRUCTURE AND CREEP IN Sn-3.8Ag-0.7Cu SOLDER

Orlando A. Cornejo
Lieutenant Commander, Chilean Navy
B.S., Chilean Polytechnic Academy, 1993

Submitted in partial fulfillment of the requirements for the degree of

MASTER OF SCIENCE IN MECHANICAL ENGINEERING

from the

NAVAL POSTGRADUATE SCHOOL
September 2007

Author: Orlando Cornejo

Approved by: Indranath Dutta
Thesis Advisor

Anthony Healey
Chairman, Department of Mechanical and Astronautical Engineering

THIS PAGE INTENTIONALLY LEFT BLANK

ABSTRACT

Solder joints provide mechanical and electrical interconnections between electronic devices and packaging substrates in electronics applications. The different coefficient of thermal expansion (CTE) between substrate, silicon device and solder imposes strains on the solder joint. Creep constitutes the primary deformation mechanism, limiting the low cycle fatigue life of solder joint. The trend toward miniaturization, higher service temperatures, and higher current densities and the transition to lead-free solders, which possess higher melting points than leaded solders, aggravate the situation. Therefore, the knowledge of properties and performances is needed to be able to predict the lifetime of solders in order to assure successfully applications in electronic assemblies. This study focuses on the change of microstructure due aging in bulk and ball joints, and a preliminary analysis of the primary creep behavior of Sn-3.8Ag-0.7Cu. Differences in microstructure evolution between bulk and small joints are highlighted.

THIS PAGE INTENTIONALLY LEFT BLANK

TABLE OF CONTENTS

THIS PAGE INTENTIONALLY LEFT BLANK

LIST OF FIGURES

LIST OF TABLES

THIS PAGE INTENTIONALLY LEFT BLANK

ACKNOWLEDGMENTS

I would like to acknowledge the help, guidance and encouragement from my advisor, Dr. Indranath Dutta, and for his patience and understanding in guiding me through this work. I would like also to acknowledge the help and support from Dr. Sarath Menon for his invaluable assistance in Microscopy, and Dr. Praveen Kumar for several hours of technical discussions.

I also gratefully acknowledge the collaboration of Mr. Dhruv Bhate and Professor G. Subbarayan of Purdue University, who supplied the microelectronic solder joints aged to different extent, as well as the primary creep data for analysis.

I would like also to thanks my wife Paula and my children Sebastian, Valentina and Beatriz, all of whom understood the importance and need for all the time and weekends spent at school. They were my priceless support to achieve this goal.

Finally, the financial support of this program from the Semiconductor Research Corporation is gratefully acknowledged.

A la Virgen del Carmen, Patrona y Generala de las F.F.A.A. de mi Patria.

THIS PAGE INTENTIONALLY LEFT BLANK

I. INTRODUCTION

Solder joints were initially intended to be simple electrical interconnections between mechanically interconnected components in electronic packages providing electrical, mechanical and thermal continuity between electronics components [1]. Therefore, the use of Sn-Pb solder was widespread due to several advantages, such as low cost, good manufacturability, and good wettability on common substrate such as Cu and Ni used by the Electronic Industry. During the 1980s, surface mount technology (SMT) was used to attach electronic devices, like resistors or chips, to a printed circuit board (PCB) without the aid of holes, permitting the increase of electrical connections per integrated circuit chip [1,2]. One of the most common methods of connection is via the use of Ball-Grid Arrays (BGA), which consists of 500-800 μm diameter solder balls that provide mechanical and electrical connection between electronic substrate and PCB as depicted in Figure 1.

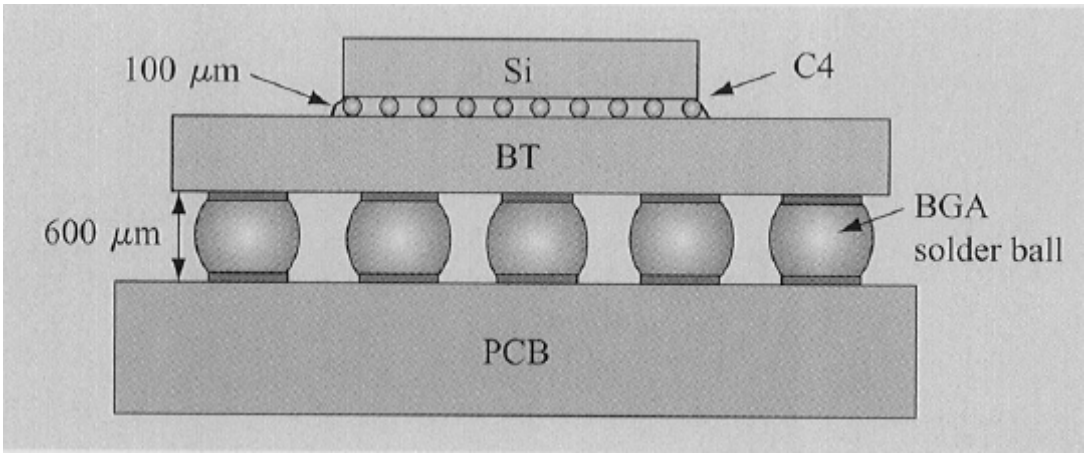

Figure 1. View of a Package Assembly [15].

Considering that the individual components joined in an electronic package have different thermal expansion coefficients, a key issue in long term reliability of solders is joint failure during thermal cycling due to powering on/off. When the assembly undergoes a change in temperature, a thermally induced strain is imparted to the solder joint [1]. The failure, electrical open circuit, of a single solder joint could mean the failure of the assembly. Moreover, with the increasing number of joints per package and the service environment becoming more severe, the reliability of solder under conditions of thermomechanical fatigue becomes more critical. Under aggressive thermomechanical cycling with high homologous temperatures (T_m), creep constitutes the primary deformation mechanism, and limits the low cycle fatigue life of solder joint, and hence the entire microelectronic package [7, 9, 10].

The situation becomes more severe with the increasing device miniaturization, less weight, increase power generation and hence operating temperatures, which tend to decrease solder balls size even more [5], hence, more severe service environments impose superior performance and high reliability on solders. Moreover, during thermomechanical cycling (TMC) and service at high homologous temperatures, solders undergo a rapid strain-enhanced coarsening [5, 11, 12], resulting in an in-service evolution of the creep response. Quite often, reliability issues are linked to microstructural evolution of solder joint materials. Microstructural evolution at high temperatures may have detrimental effects on joint integrity [13, 18]. Amongst several causes for the microstructural evolution can be

named natural or artificial aging, differences in cooling rates and strain-enhanced coarsening due to TMC [12, 13].

Despite the advantages exhibited by the Sn-Pb solders, global economic and environmental pressures tend to discard the use of Pb. As an example, the European Community (EC) issued the Waste of Electrical and Electronic Equipment mandate that aimed to prohibit the use of Pb-Sn solders by year 2006 [2]. Under legislation pressure and trade competition, large electronics manufacturers and research institutes studied a replacement for these types of solders. Amongst the studies, the Lead-Free Sn-Ag and Sn-Ag-Cu are promising candidates as replacing solders. The major advantages for that are the higher melting point (T_m=217-220^{0}C), which provide a higher range of operational temperature; comparable wettability with the Pb-Sn solder on copper substrate; and good mechanical properties [5, 13, 14]. However, since the reliability of solder rests on its capability to withstand creep, a second phase is introduced in the soft Sn matrix in an effort to improve properties such as thermo-mechanical fatigue resistance, creep resistance, and mechanical strength [13].

For the present thesis, Sn-3.8Ag-0.7Cu (SAC-387) was the selected material, where the objectives of the present work are (1) to study the effects of aging in microstructure with particular attention in natural aging, and (2) the effects of microstructure changes on creep behavior of the solder.

THIS PAGE INTENTIONALLY LEFT BLANK

II. BACKGROUND

A. MICROSTRUCTURE OF SN-3.8AG-0.7CU

The structure of Pb-Sn solders has been widely studied, and consists of equiaxed grains of Pb-rich and Sn-rich phases, both of them coarsen. This affects the diffusional creep component only, without any effect on dislocation creep. On the other hand, microstructure of Sn-Ag and Sn-Ag-Cu solders typically consist of dispersed intermetallics in a β-Tin matrix, the grain size of which is considerable relative to joint size. This minimizes impact on diffusional creep. The primary coarsening effect in solders arises from the rapid coarsening of intermetallics particles, been the dislocation-creep component the dominating creep mode. [12]

It has been shown that it is energetically favorable for a two phase structure whose minor phase has a volume fraction greater than 0.28 to form a lamellar structure; conversely, for volume fractions less than 0.28, a rod-like morphology has the minimum interfacial energy. An increase in volume fraction for a lamellar structure only increases the thickness of one phase without change in surface area. On the other hand, for a rod-like structure, an increase in volume fraction does mean an increase in surface area. Although this approach holds for many systems, if an orientation relationship exists between phases, the critical volume fraction at transition will shift. Therefore, for a binary eutectic system its morphological nature can be predicted from the knowledge of the relative volume fraction of phases at eutectic composition by using the inverse lever rule and the phase diagram. [20]

Considering the above statement, it can be said that microstructural configuration is going to be function of volume fraction [20] and cooling rate [23]. That means that an increase in volume fraction will decrease the steady-state creep rate. On the other hand, an increase in cooling rate decreases the time necessary for diffusion, resulting in a finer dendrite microstructure of β-Sn and promoting spherical and finer intermetallics particles [23] which decrease the steady-state creep rate also.

Fix et al., [17], Lewis et al., [20], Moon et al., [21] amongst others studied the ternary phase diagram for Sn-Ag-Cu. The ternary eutectic reaction in SnAgCu results in decomposition of melt L into three solid phases:

$$L \longrightarrow \beta\text{-Sn} + Ag_3Sn + Cu_6Sn_5$$

For that reaction, it has been reported a eutectic temperature of 217^0C and a composition of 4.7%Ag-1.7%Cu-93.6%Sn [17, 21], which is close to the solder composition of the present study.

Since ternary eutectics are mixtures of three phases, it is expected to find a larger number of morphological classes than binary eutectic, which can be described as combinations of fibrous and lamellar phases. The resultant ternary structure depends on three solid-solid and three solid-liquid interfacial energies and two volume fractions. A Sn-Ag-Cu phase diagram assuming equal interfacial energy between all phases as depicted in Figure 2. As an analogy for binary eutectic, for equal interfacial energy and a small volume fraction, a rod-like morphology would be expected for a ternary eutectic. [20]

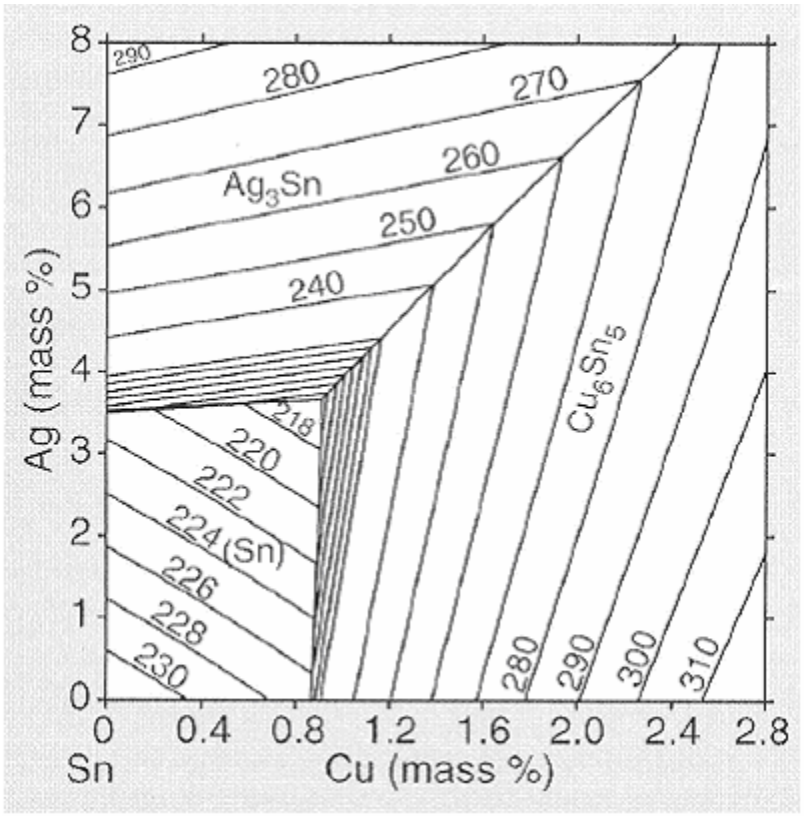

Figure 2. Updated Phase Diagram Ag-Cu-Sn [21].

It is noteworthy that the eutectic composition contains about 95% Sn, which suggest that the physical, chemical and mechanical properties of the solder is going to be heavily influenced by properties of pure Tin. Pure Tin is polymorphic and capable of existing in three crystal structures (α,β,γ), where white-Tin phase (β) has a body-centered tetragonal (BCT) crystal structure, which explain is less isotropic mechanical and physical properties compare to Pb [15]. The near eutectic composition Sn-3.8Ag-0.7Cu upon solidification consists of a complex pure β-Sn dendritic arm structures surrounded by a network in which the all three phases are interspersed. Depending on composition and cooling rate, in the interdendritic regions

consists of large pro-eutectic particles of Ag_3Sn and Cu_6Sn_5 [15, 17]. A rapid cooling rate resulted in a decrease in the secondary dendrite size, as well as the secondary dendrite-arm spacing, which is because of the decreased time for diffusion. The rapid cooling rate promoted nucleation but suppressed the growth of Ag_3Sn, yielding a fine and spherical morphology [23]. On the other hand, a slower cooling rate, allowed more time for diffusion to occurs, yielding a larger plate or rod-like Ag_3Sn morphology and Cu_6Sn_5 also [23].

The formation of this dendritic microstructure is an indication of non-equilibrium solidification during the solder formation [15], which means that this metastable structure can be destabilized at room or high temperatures due to high interfacial energies.

At room temperature (25^0C), which means 0.6 T_m (where T_M=Melting Temperature), diffusion mechanism dominates, meaning that under isothermal aging conditions, the intermetallic particles size coarsen and spacing amongst them increase [11]. However, during the spreading and coarsening of the eutectic structure, Cu_6Sn_5 particles increase its size larger than Ag_3Sn, which is consistent with the higher diffusivity of Cu in Sn than Ag in Sn [7].

During TMC, particles experienced both static and strain-enhanced coarsening, increasing their size and increasing its spacing. It has been reported that the extent of strain-enhanced coarsen is significantly greater than due static aging only [11].

As stated, static and strain-enhanced coarsening has a detrimental effect, since the coarsen particles could became

so large and spread that they can not longer being an obstacle for dislocation. They also provide a site where cracks can initiate and grow, meaning the failure of the assembly [11, 13, 18, 23].

B. MICROSTRUCTURAL EFFECTS ON MECHANICAL BEHAVIOR

Since the homologous temperature exceeds 0.6 (room temperature) at the operating point for most solder alloys, thermally activated creep plays an important role in deformation behavior of solders, being creep fatigue the more prone way of failure in solder joints [22]. Therefore, an understanding of the dependence of mechanical properties on the microstructure is of considerable interest [16, 24].

There are two common creep tests performed on solder joints: stress rupture and stress relaxation test. In case of stress rupture, the load is held constant and the stress is recorded as a function of time. On the other hand, in stress relaxation test, the sample is loaded to a specific stress and then held at a constant displacement, while relaxation of load is recorded [5]. The data collected are of extreme importance to estimate the strain experienced by the samples. It is well known that the values obtained for steady state rate, stress exponent and activation energy (Q) typically represent the dominant creep mechanism [25].

One of the most important processing variables that control the solder microstructure is cooling rate, because directly affects the microstructure of solder, hence affect mechanical behavior. Ochoa et al., [23] amongst several others authors, stated that increasing cooling rates decreased the Sn-rich phase secondary dendrite-arm and

spacing. Faster cooling rates, promotes nucleation but suppressed growth of Ag_3Sn, yielding a fine spherical dispersed morphology. Conversely, slower cooling rates resulted in needle-like AG_3Sn. However, cooling rate did not affect the Young's Modulus of the solder, which is highly affected by the fraction of porosity in the solder [23]. Based on result of Sigelko et al., [19], the dendrite size, orientation, and randomness do not significantly affect the mechanical properties of solder joints.

The key microstructural feature of Sn-based Pb-free solder alloys is the presence of intermetallic phase's particles. The influence of low volume fractions of precipitates on the creep performance and associated strengthening effects is recently recognized [26]. Comparison of creep test amongst of several solder alloys gave the following order of creep resistance from least to greatest:

Sn-37Pb < Sn-0.7Cu < Sn-3.5Ag < Sn-3.8Ag-0.7Cu [22]

The ranking is explained by the fact that the concentration of intermetallic increases with the concentration of alloying elements [22]. Even more, Kerr et al.,[27] studied the creep behavior of pure Sn compare to Sn-3.5Ag stating that the intermetallic particles of Ag3Sn strengthen the Sn matrix, causing the material to behave as a dispersion strengthened metal [7,29].

The precipitation of second-phase particles throughout the matrix increases the difficulty of dislocation motion through the lattice, regarding that the volume fraction, distribution, nature of precipitate and nature of intherphase boundary are accomplished [28]. Considering that

the IMC in the solder are harder that the matrix and they possesses a coherent interface, dislocations are forced to loop around them. That dislocation looping mechanism provides a measure of strain hardening, and it is controlled by the spacing between particles. It is often referred as *Orowan* looping [28]. Furthermore, aging increase size and spacing of particles, leading also to the diminishing of coherency, this means a decrease of alloy strength and creep resistance [28].

Pan et al., [7], Dutta et al., [11] amongst several authors studied lead-free solders creep behavior and microstructure. All of them stated that is a distinctly low and high stress regime, displaying a clear mechanism transition. At low stresses the stress exponent (n) found was around 6.0, where deformation is slow and creep is controlled by general climb of dislocations segments around particles. At high stress an apparent stress exponent (n_{app}) of 7.5-9.5 was determined [7,11], where the rapid deformation rate permits climb of large dislocations segment, allowing only local climb of short segments over particles, which is named particle-limited climb [11]. It was also determined that the stress exponent and activation energy (Q) for pure Sn is n=5 and Q=42 KJmole respectively, which with the increase of alloying elements is increased as n=6 and Q=62 KJmole. That shown an increasing effect of particles controlling creep due dislocation climb through eutectic.

Other approach to improve reliability is using composite solder, which consist of a solder matrix and reinforcements. The reinforcing particles can suppress

grain-boundary sliding, intermetallic compound formation, grain growth and redistribute stress uniformly [30]. The modified solder should function similar to monolithic solder by appropriately demonstrating good wetting on substrate, proper flow characteristics, and reliable bonding [18]. This can be achieved by fine, dispersed Cu_6Sn_5 intermetallic particles. The presence of these particles could come from the composition of the solder or by diffusion from the Copper substrate into the solder joint. The addition, intentionally or unintentionally, of these particles tended to limit the size of dendrites while they form [19]. At low strain rates, composite solders possesses better creep resistance compare to non-composite solder; but under more rapid deformations conditions, its behavior resembles the non-composite solders [18,22,31].

Gou et al., [31], Subramanian et al., [18] prove that the Cu_6Sn_5 particles have a weak interface bonding, which can not provide significant load transfer to the reinforcement, thus, only a modest increase in strength is expected. However, the weakly bonded interface does enhance ductility by stimulating deformation more uniformly throughout the solder joint [18]. Very little coarsening of the Ag compare to Cu particles is observed, which is related to the differences of diffusivity of Cu and Ag in Sn, being Cu in Sn 1000 times faster in BCT than does Ag. Therefore, is attributable the main strengthening and creep resistance, due is larger volume fraction and smaller size, to the Ag_3Sn particles [7, 18, 22, 29].

III. EXPERIMENTAL PROCEDURE

A. SAMPLE FABRICATION

1. Solder Samples Procedure

The samples were constructed from an ingot obtained from *Freescale Semiconductors*. The major characteristics and composition of SAC-387 are depicted in Tables 1 and 2 and fabrication procedure as follow:

SAC 387	
Sn	Balance
Ag	3.8 +/- 0.2
Cu	0.7 +/- 0.1
Pb	0.1 max.
Sb	0.10 max.
Zn	0.001 max.
Fe	0.02 max.
As	0.03 max.
Ni	0.01 max.
Bi	0.1 max.
Cd	0.001 max.
Al	0.001 max.
In	0.05 max.

Table 1. SAC-387 Specification [6]

SAC 387	
Melting Point	217-219 ^{0}C (423-426 ^{0}F)
Density	7.44 grs/cm^3
Specific Heat Capacity	0.236 J/g^{0}K
Hardness	14.9 HV

Table 2. Materials Characteristics [6].

- Roll solder rod down to about 1 mm thick foil, cut to about 4 mm wide strips. Load them into the graphite mold.

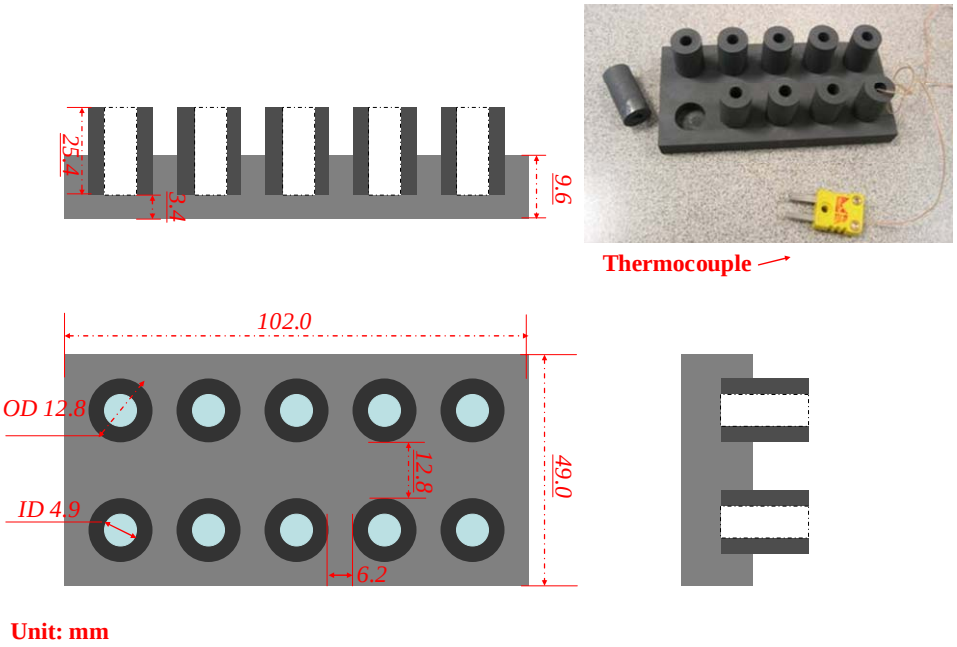

Figure 3. Graphite Mold.

- Heat furnace to 260 ^{0}C and wait for 20 minutes to homogenize temperature. Flow Nitrogen gas through furnace to minimize oxidation.
- Place an aluminum plate on an aluminum container and fill with liquid nitrogen at a level a little below of aluminum plate as depicted in Figure 4.

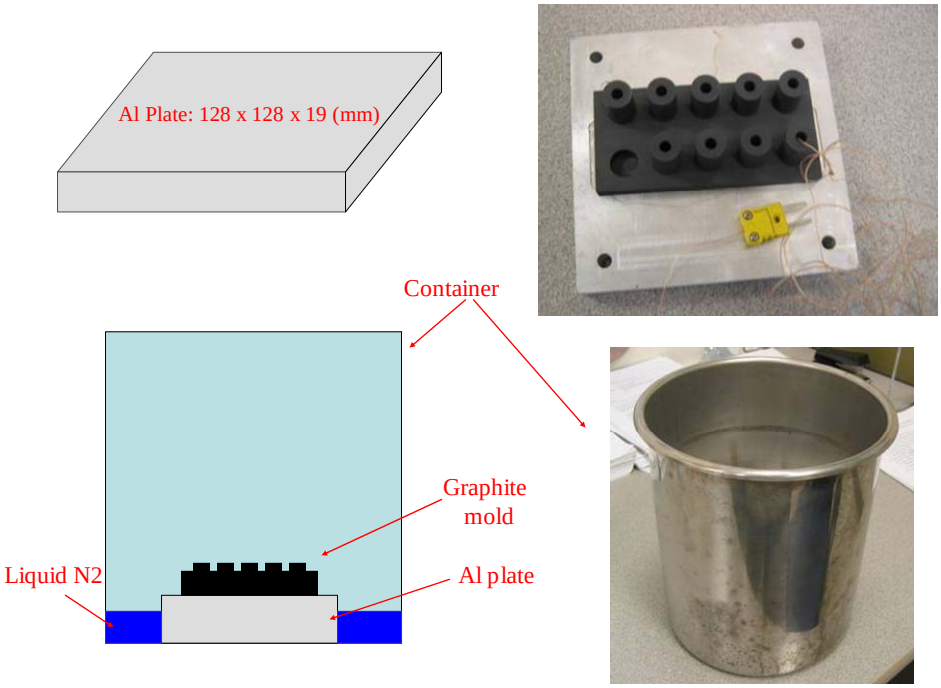

Figure 4. Aluminum plate and container.

- Place the graphite mold (depicted in Figure 3) filled with SAC into the furnace, flowing nitrogen gas into furnace. Dwell time at temperature was 10 minutes controlled by a K type Thermocouple and stop watch, to assure is completely melted.

- Take out the mold quickly and placed on the aluminum plate, assuring that the liquid Nitrogen level is a little below the plate surface (As depicted in Figure 4).
- Sample cooled to 130 ^{0}C in one minute using thermocouple and stop watch.
- Cooled cast samples were approximately 15 mm long and 4.9 mm in diameter. For cutting a die (depicted in Figure 5) was used to dimension them to 5 mm long approximately, by using a slow diamond saw.

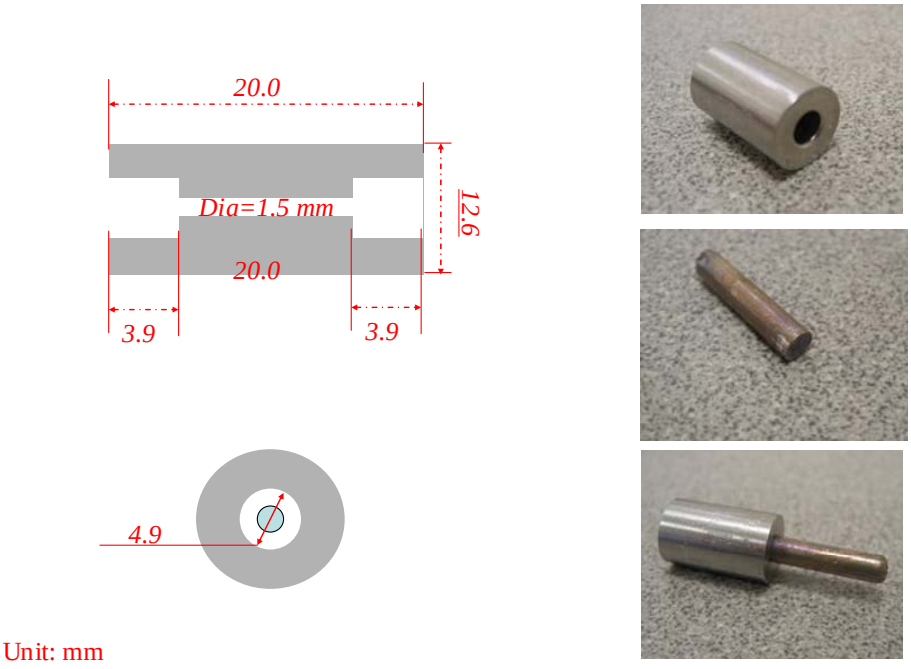

Figure 5. Die for cutting samples.

- After cutting and in order to flatten and make parallel both surfaces of sample rods before testing, a Die (depicted in Figure 6) was used to

hold the sample while a 1000, 2400 4000 Silicon Carbide Paper, with water as lubricant, was utilize.

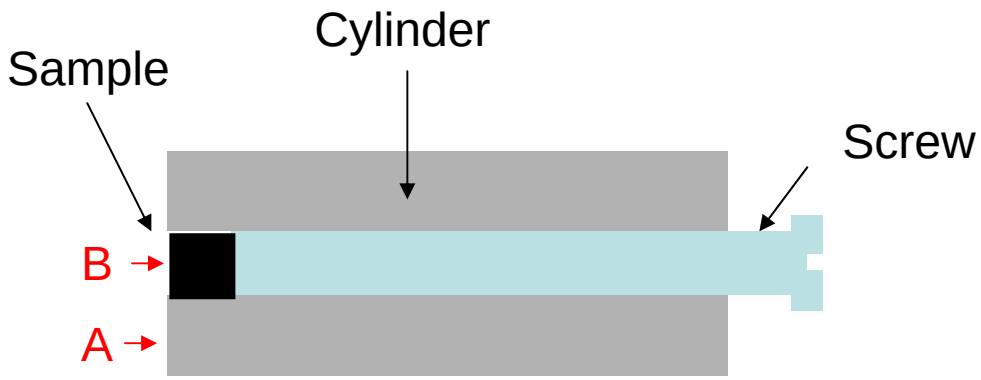

Figure 6. Die for polishing samples.

B. APPARATUS FOR CREEP TESTING

As a Creep Testing machine was utilized a *MTS 858 Table Top System with Teststar II's Controller Setup Version 3.2*. The *System Software Model 793.00* was utilized for programming test procedures. A standard 3 stages program was utilized for the tests using a 10 KN load cell:

- *Initial Approach*, were the hydraulic ram approach to the specimen at 0.1 mm/sec until -2 N was sensed, following by *Hold* the load for 5 minutes to provide enough time to temperature to stabilize after touching the sample. The data points were selected each 0.5 seconds to provide enough data points.

- *Loading* stage, were the load was increased in a ramp 1 N/sec until reaching the desired load,

which are depicted in Table 3. Data were obtained each 0.5 seconds also, providing enough data points to calculate the initial displacement (δ_0) of samples after reaching desired load.

- Compression *Test* which kept a constant load for 48 hr. The program was accomplished at several different load values (Table 3) and recorded Time, RAM displacement, Temperature and Load every 10 seconds, in order to get enough data points to analyze the curves. A Test at 100^{0}C is depicted in Figure 7 as an example.

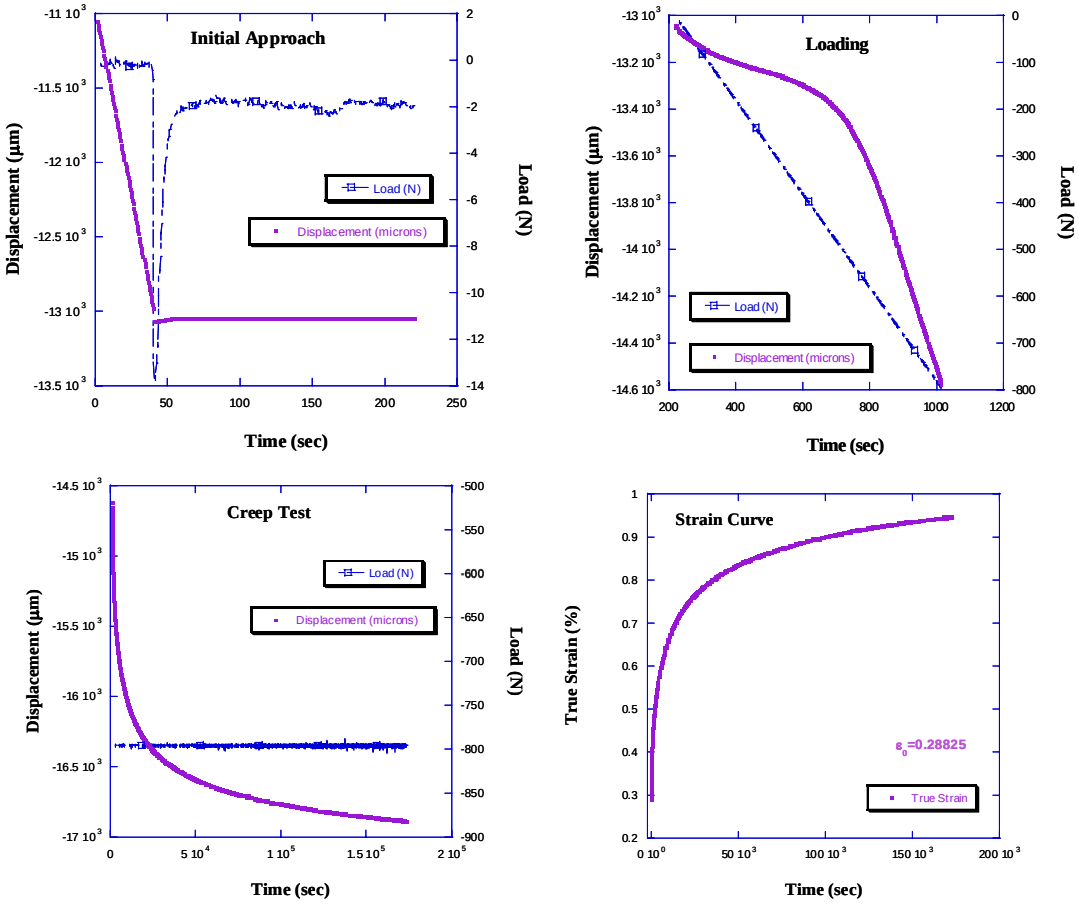

Figure 7. 42.2 MPa-100^{0}C-48 hrs Test.

The test procedures were accomplished at 3 different temperatures: 323^0K, 373^0K, and 423^0K (50^0C, 100^0C, 150^0C). That for an *Omega I Series Temperature/Process Controller Model CNI18A33-Vi7* was utilized to set and kept a stable temperature to the furnace and to grant the proper temperature record on the program of *MTS* machine.

C. EXPERIMENTAL PROCEDURES AND RESULTING CURVES

A first step for experimental procedures was the selection of the proper target load selection and temperature. Considering a previous work of Pan et al., [7], two stress data points at low stress and two at high stress were selected, using the same temperatures from his work, which are depicted in Table 3.

Temperature ^{0}K (^{0}C)	STRESS (MPa)	LOAD (N)
323 (50)	18.7	352.6
323 (50)	25	471.4
323 (50)	43.7	824
323 (50)	50	942.8
373 (100)	11.2	211.2
373 (100)	15	283
373 (100)	33.7	635.5
373 (100)	42.2	795.8
423 (150)	15	282.9
423 (150)	25	471.4
423 (150)	35	660

Table 3. Testing Stresses-Temperatures.

The samples obtained after reflow and before testing were polished, with silicon sand paper until 4000 grit, by using the polishing kit (Figure 6) on both ends to assure parallelism and using graphite film as a lubricant to diminishing friction factor. That does will ensure to avoid errors caused by friction between loading platens and sample errors caused by sample barrel deformation. The stage and rod of MTS machine were verified with a spirit level to ensure parallelism amongst rod, sample and stage also. A couple of ceramic pieces were placed above and below from the samples to avoid heat conduction through the stage or

rod that can affect the load cell of *MTS* machine. A general view from the sample assembly is depicted as Figure 8.

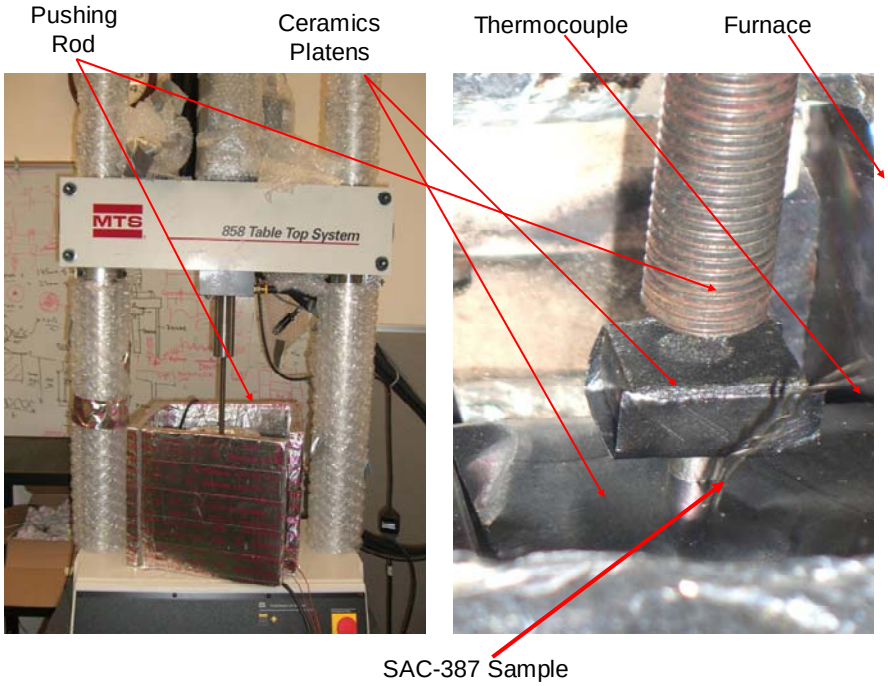

Figure 8. General View of Test assembly.

The program was settled to obtain Time, Displacement (μm), Load (N)and Temperature (Celsius) in intervals of 10 second between each data point for the 48 hours Creep Test. From data extracted and using the following formulas [28]:

Engineering Stress $\sigma_{eng} = Load / Initial\_Area$

Engineering Strain $\varepsilon_{eng} = Displacement / Initial\_length$

True Stress $\sigma_{True} = \sigma_{eng}\left(1+\varepsilon_{eng}\right)$

True Strain $\varepsilon_{True} = \ln\left(1+\varepsilon_{eng}\right)$

was possible to calculate and plot the True Strain against Time for each sample tested. Considering that in a compression test the sample is continuously increasing its area due deformation from the applied load (Target Load), hence the True Stress drops continuously. From True Strain vs. Time Curve, the Steady Strain Rate ($d\varepsilon/dt$) and the True Stress were obtained, data which was necessary to calculate the Stress Exponent (n) and Activation Energy (Q) for Creep, knowledge which permits us to understand the dominant creep mechanism operating. True Strain Curves at 50^0C, 100^0C, and 150^0C are depicted in Figures 9, 10, and 11 as an example.

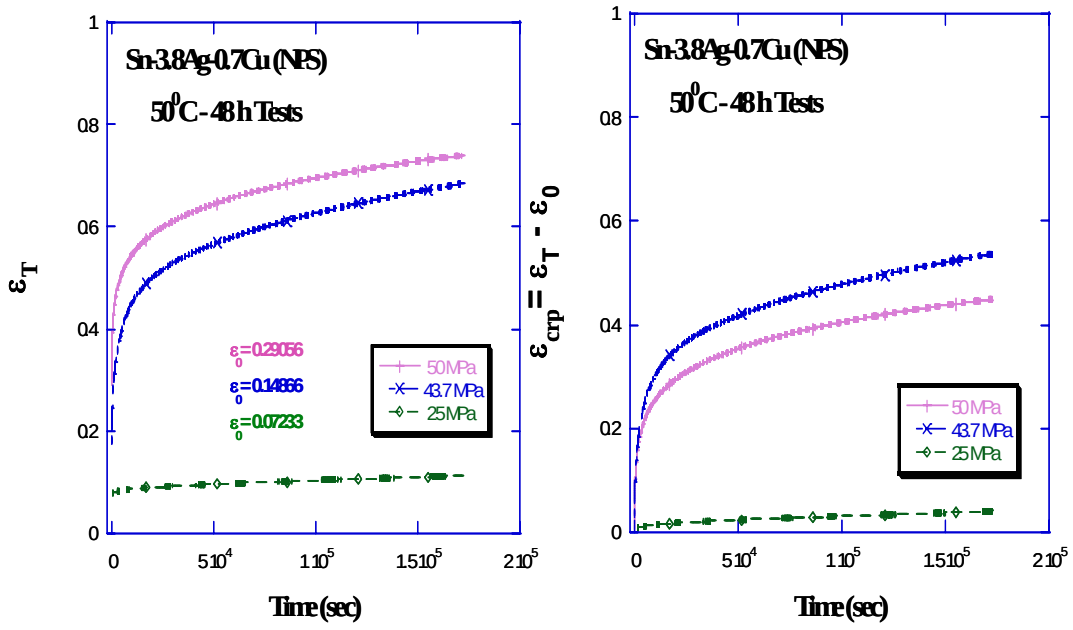

Figure 9. Test at 50 Celsius.

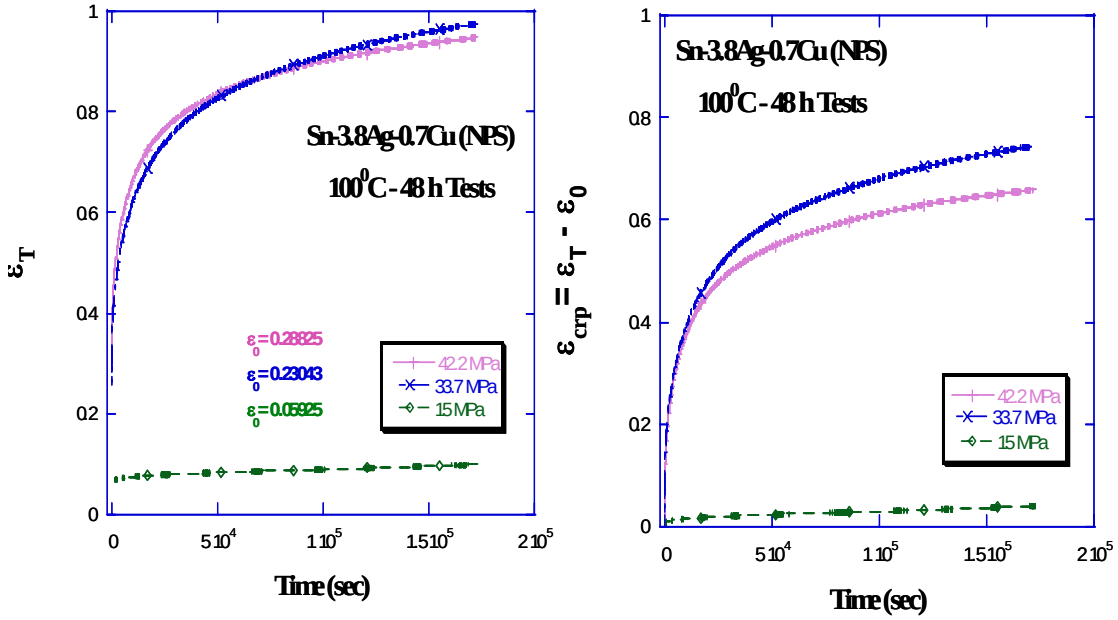

Figure 10. Test at 100 Celsius.

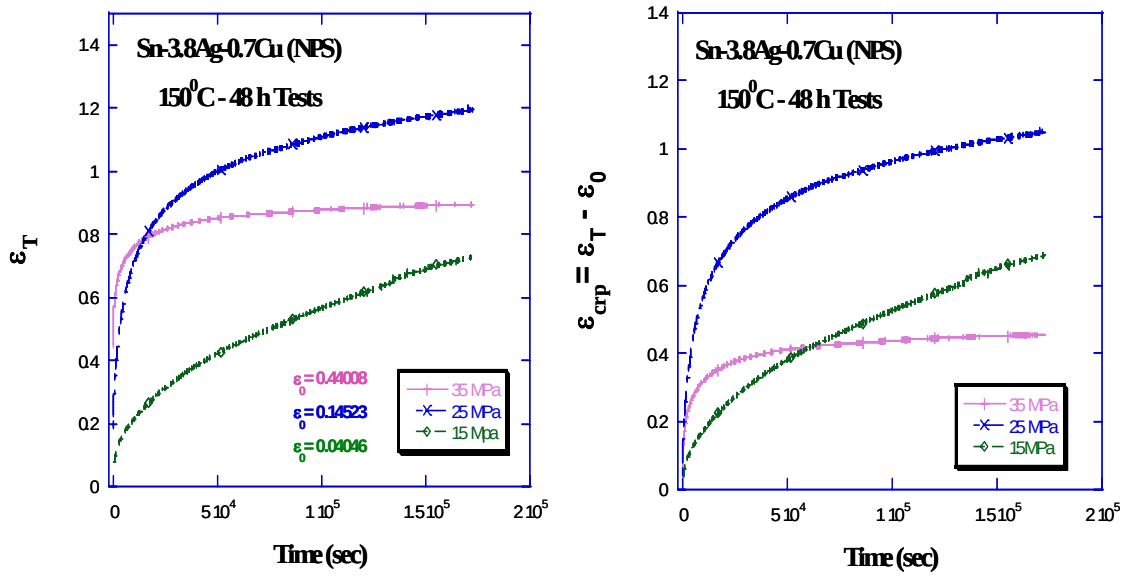

Figure 11. Test at 150 Celsius.

D. METALLOGRAPHIC PREPARATION

1. Bulk Cylinders

- Considering that samples were tested in compression at several stress levels, their appearance was very flat. In order to prepare them for metallography, tested specimens were held longitudinally with *Buehler Sampl-Klip (Part Number 20-4000-100)* and mounted in one part of *Buehler Sampl-Kwick Liquid (Part Number 20-3568)*, two parts of *Buehler Sampl-Kwick Powder (Part Number 20-3566)*, one part of *Buehler Conductive Filler (Part Number 20-8500).*
- After mounting, the samples were polished in steps with 1000, 2400, 4000 Silicon Carbide Paper, in order to remove scratches from the previous stage, utilizing tap water as a lubricant, rinsed with water, sonic cleaned for five minutes, and rinsed with methanol between each step. It is important to note, that due the softness of solder, grinding was done on a stationary wheel by hand.
- Using minimal force, polishing in a stationary *8" Buehler Microcloth PSA 10/PK (Part Number 40-7218)* with *Buehler* $3\mu m$ *MetaDi Monocrystalline Diamond Suspension (Part Number 40-6531)* for three minutes.
- After rinsing with water, sonic cleaning for five minutes, rinsing with methanol, using the same kind of cloth in a stationary wheel, a Buehler

$1\mu m$ *MetaDi Monocrystalline Diamond Suspension (Part Number 40-6530)* was utilized for three minutes, followed by rinsing in water, sonic cleaning, and rinsing in methanol.

- Final polishing used *Buehler Mastermet Colloidal Silica Polishing Suspension (Part Number 40-6370-064)* for two minutes following by rinsing, sonic cleaning, rinsing with methanol and drying with hot air.

2. Ball Joints

For Ball Joints, the same procedure described in previous section for metallographic preparation was used with the same solution, cloth and Silicon Carbide Paper. However, the best polishing results were achieved polishing only along the long axis of silicon plates.

E. MICROSTRUTURAL CHARACTERIZATION OF SN-3.8AG-0.7CU

After mounting and polishing a sample by the procedure already described, an As-reflowed sample (SAC-387) was characterized by the aid of an optical microscope *NIKON EPIPHOT 200* and micrograph using a Scanning Electron Microscope *TOPCON SM-510.*

From the ternary phase diagram [17,21] and considering the volume fraction and rapid cooling rate imposed to samples, was expected to obtain a Primary β-Tin dendrites surrounded by a fine dispersion of precipitates of Ag_3Sn and Cu_6Sn_5 as depicted in Figure 12. It can be seen that the dendrites are large in size compared with an interdendritic

eutectic of fine particulates. Micrograph depicted as Figure 13 shows at higher magnification the dendrites and the particulates at the interdendritic area.

Considering that the creep resistance of the solder depends on the size of intermetallic particles, a manual measurement of particles was accomplished. For this, in each particle was assumed to be an ellipse. Therefore, a measure of its major and minor axis was done and plotted in form of a histogram and probability curve (Figure 14). A mean of 0.32024 and 0.45384 μm, and a median value of 0.30111 and 0.41963 μm, for minor and major axis respectively, were obtained.

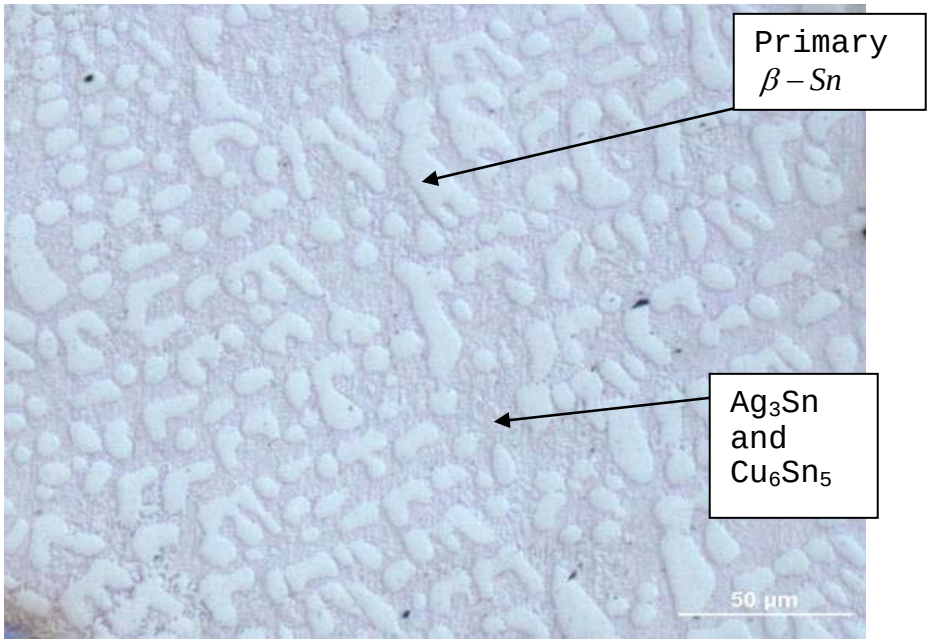

Figure 12. Optical metallography of bulk SAC-387 showing initial dendrites structure and intermetallic particles.

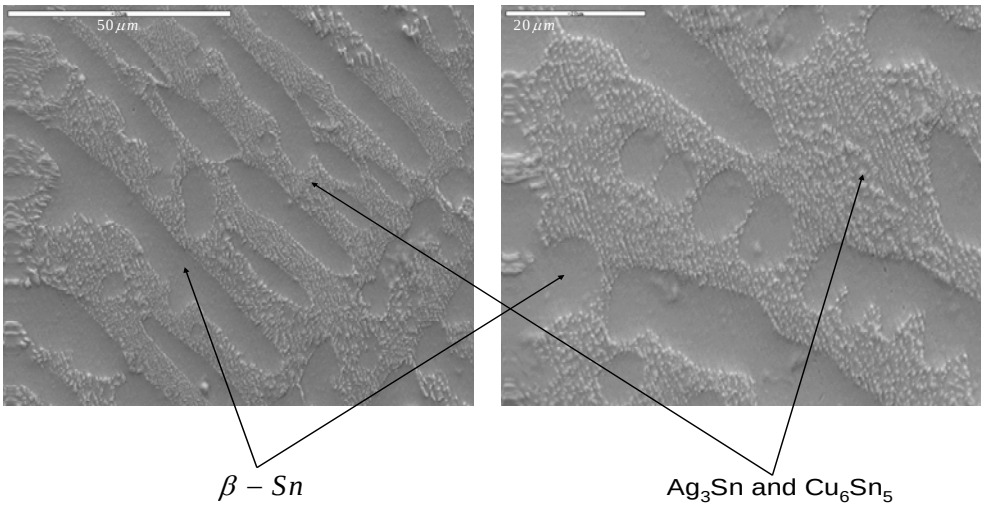

Figure 13. Micrograph of bulk SAC-387 showing initial microstructure.

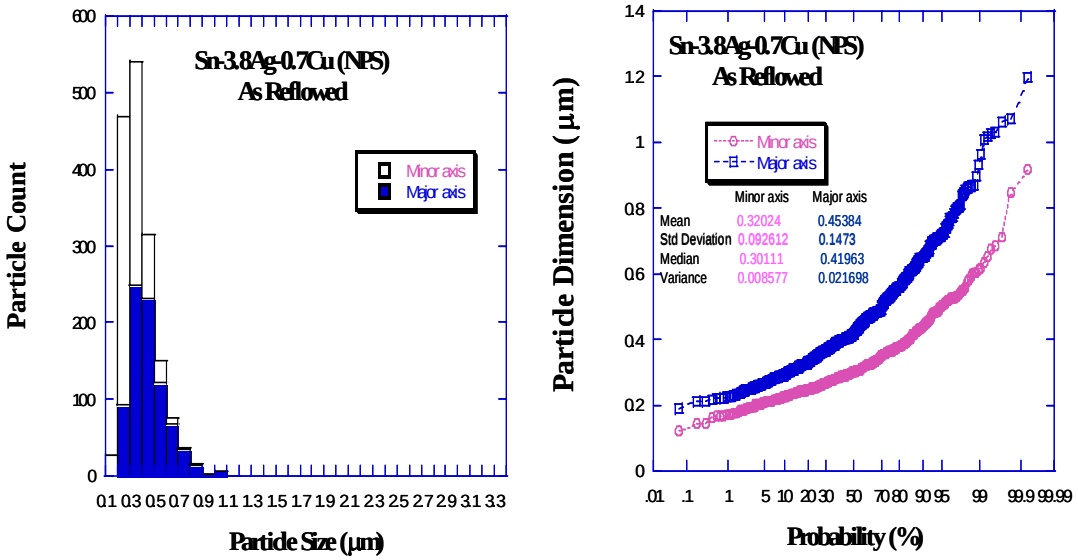

Figure 14. Histogram and probability diagram of as-reflowed.

THIS PAGE INTENTIONALLY LEFT BLANK

IV. RESULTS AND DISCUSSION

A. AGING EFFECTS

1. Natural Aging

In order to asses the effects of isothermal aging, samples of SAC-387 were aged at room temperature (25^0C or 298^0K) for six months. Considering that the melting temperature of solder is 217^0C (490^0K), room temperature represents 0.6 T_M. Therefore, some changes are expected in microstructure. From optical metallography (Figure 15) it can be seen that the Tin dendrites colonies are clearly seen, showing in the interdendritic spaces the intermetallic compound particles of Ag_3Sn and Cu_6Sn_5.

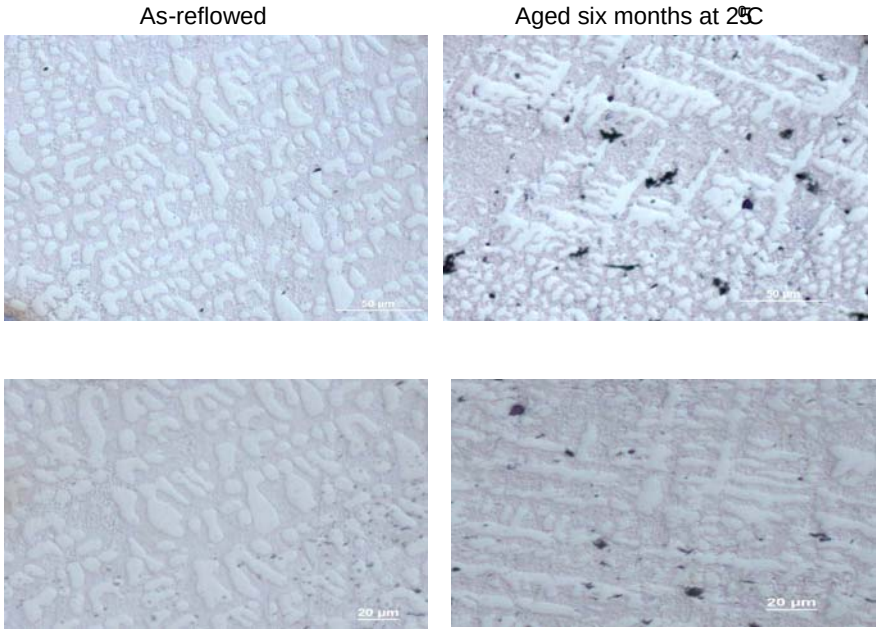

Figure 15. Comparison metallography of bulk as-reflowed vs. aged six months at room temperature samples.

A comparison between micrographs of as-reflowed and aged six months at room temperature (Figures 16), revealed the same feature where the dendrites are clearly seen. However, a high magnification micrograph (Figure 16) shows a probable coarsening of particles.

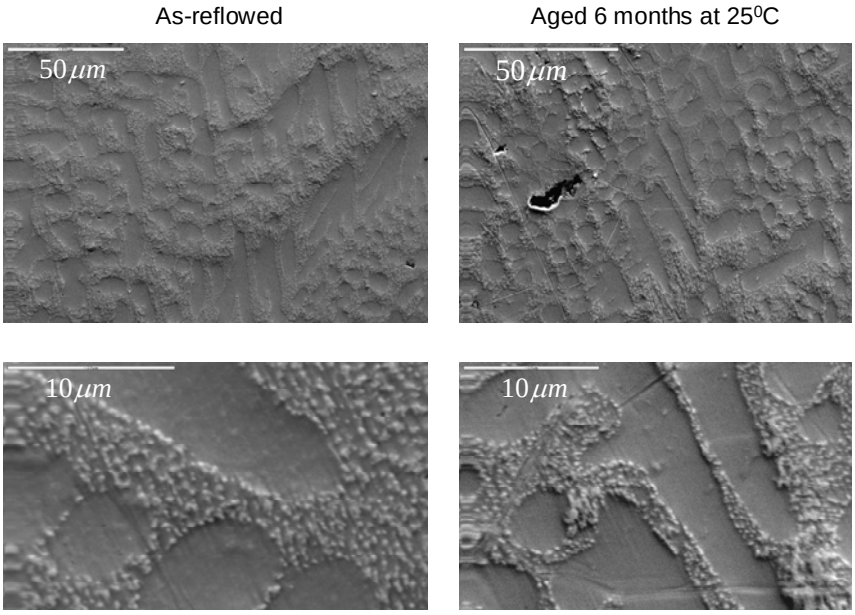

Figure 16. Comparison micrograph of bulk samples at low and high magnification.

In order to assess a probable coarsening effect due natural aging, a measurement of particles was accomplished, considering each particle as an ellipse were the minor and major axis were measured. The measurements are presented in form of a histogram and probability curve (Figure 17). A mean value of 0.51316 and 0.65904 μm and a median value of 0.50283 and 0.62939 μm for minor and major axis respectively were obtained. Comparing with values for an as-reflowed solder, it means an increase of 45.2% in mean value

and 50% increase of median value for major axis. From this values can be concluded that natural aging increases mean and median sizes of particles, but a change is its aspect ratio also, which tends to be decrease, meaning that the particles are little bit rounder.

=

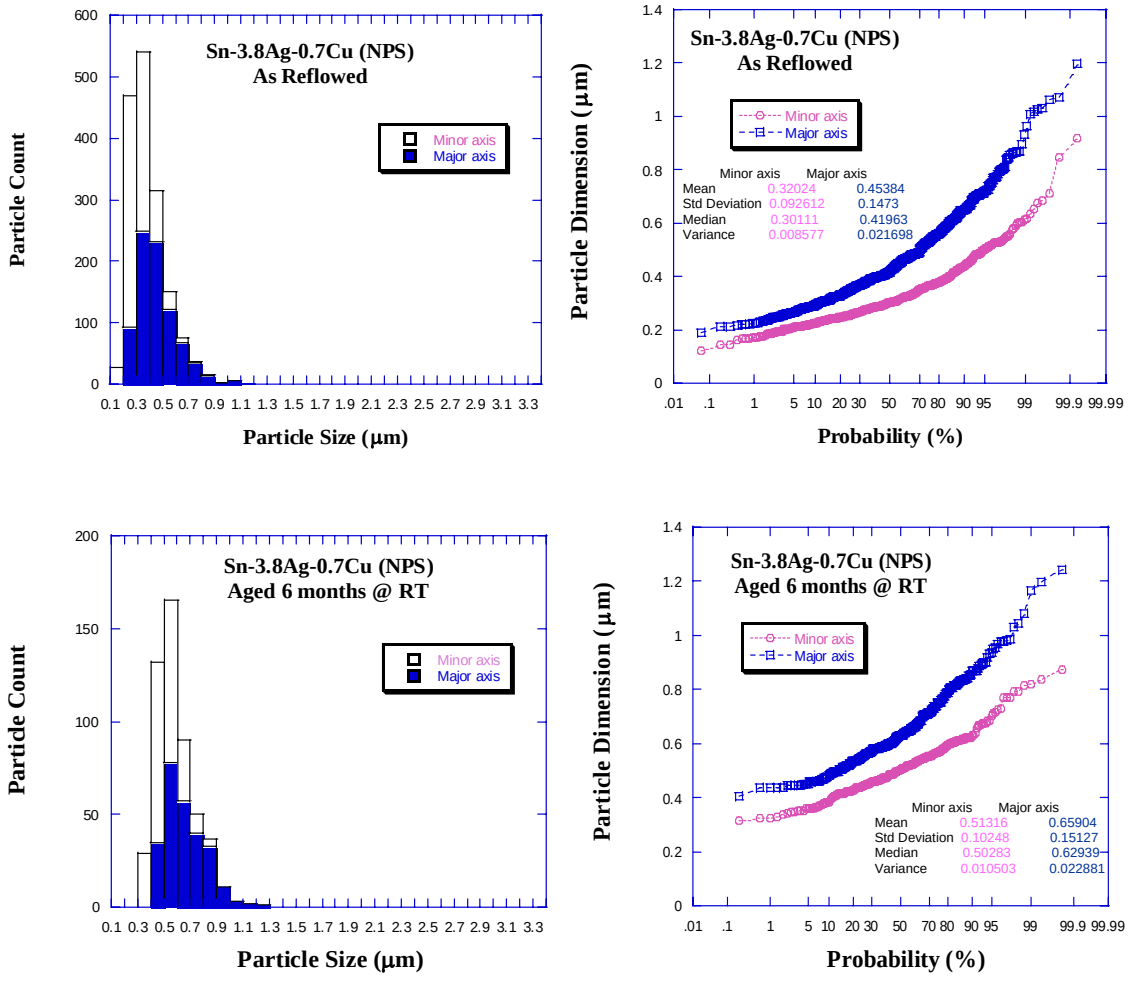

Figure 17. Histogram and probability diagram for comparison of bulk samples as-reflowed and aged six months at room temperature.

In addition to the observed increase of particle size, it is noteworthy that an increase of about 20% in the size of the largest particle is also observed. Pan et al., [7] amongst several others authors, stated that at different stages of aging, the median particle size increases, but larger particles coarsen more rapidly, resulting in an increased asymmetry of distribution, which explain the little tail seen on the histogram (Figure 17). The tail is results of a more rapidly increase of Cu_6Sn_5 particles due higher diffusivity of Cu in Sn [7], creating very small number of larger particles.

Pan et al., stated also that median value of particles provides a better fit to the cubic growth law

$$d_p^3 - d_{po}^3 = K_1 t$$

where d_p^3 is the particle size after aging, d_{po}^3 is the starting particle size, K_1 is a kinetic constant, and t is the aging time. The better fit for median is explained by the fact that the mean value is biased by few large particles of Cu_6Sn_5, whereas the median represents more closely the average Ag_3Sn particle size, which allows to track the growth kinetics of this particular particle [7]. For this particular work, it also is useful to track and compare Ag_3Sn particle size for different stages of aging using the major axis measurement.

2. Artificial Aging

In order to elucidate the microstructural effects of aging on solders, samples of as-reflowed were artificially aged in furnace at 180^0C (453^0K) for 100 hours. Considering that this temperature is 0.92 T_M and normally above

operational temperature conditions, but permit to simulate a severe coarser microstructure that resembles a strain-enhanced coarsened structure during TMC at low temperature. However, from a literature review, the microstructure is not as coarsen as that expected under normal TMC conditions [7].

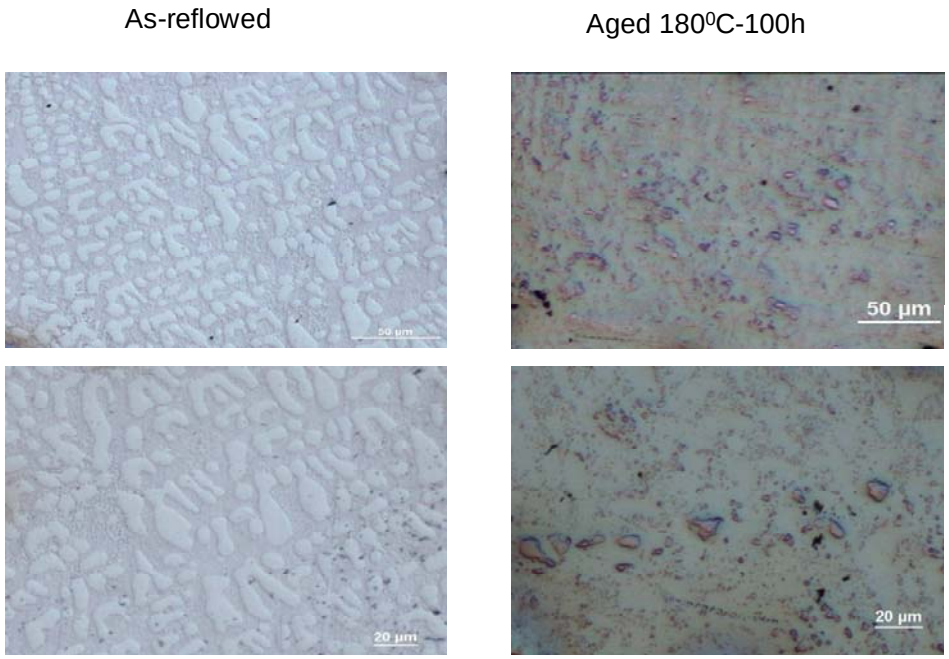

Figure 18. Comparison metallography of bulk as-reflowed vs. aged 180C-100h samples.

From the optical metallography (Figure 18) and SEM micrograph (Figure 19), it can be seen that aging leads to a loss in the definition of the dendritic structure of $\beta - Tin$ with a commensurable coarsen and spreading of eutectic structure. It shows rod-like structure; coarsen particles and minor particles dispersed in a Tin matrix, whereas diffusion is the rate-controlling mechanism of particle growth [17].

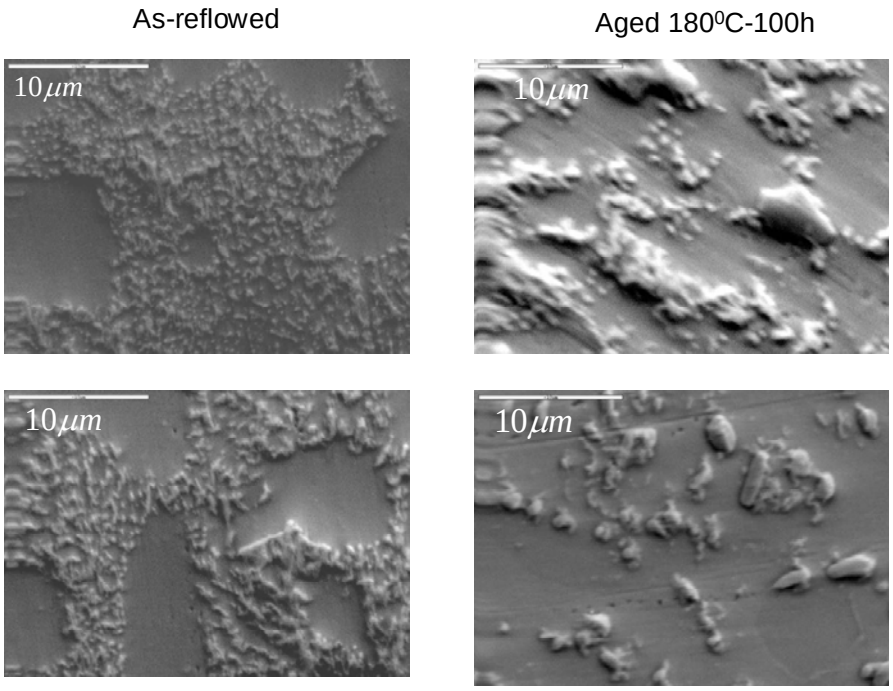

Figure 19. Comparison micrograph of bulk as-reflowed vs. aged 180^{0}C-100h at high magnification showing differences in particles coarsening.

In order to asses the particle size increase, they were measured in the same way as before, obtaining a mean value of 0.53620 and 1.0014 μm and a median value of 0.42004 and 0.79512 μm. As stated before, is noteworthy that the increase in mean value is 120.7% and median 73.2% comparing the major axis with an as-reflowed sample. A comparison with an aged six months at room temperature sample gives a mean increase of 52% and a median increase of 15.5%. As stated before, mean values are highly affected by few but larger particles which explain the long but small particle count tail of histogram (Figure 20). Again, this is due the higher diffusivity of Cu in Sn compare with Ag in Sn.

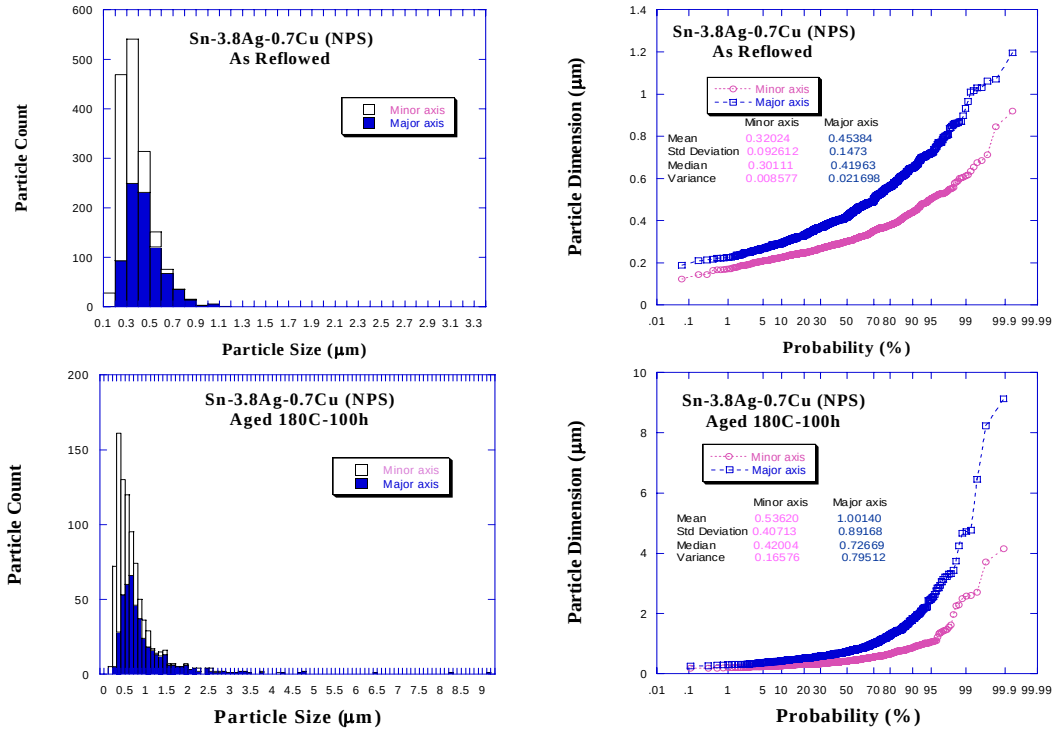

Figure 20. Histogram and probability comparison of as-reflowed vs. aged 180^{0}C-100h.

A closer look at median values, which permits to track Ag_3Sn particles in a better manner [7], can be seen that the artificial aging has a tremendous impact in coarsening of this particles, compare with as-reflowed, increasing they spacing yielding in a dramatically decrease in yield strength and work hardening rate [8]. This is due the composition of soft Tin matrix and harder eutectic particles which control the creep behavior of the alloy, therefore coarse and evenly dispersed particles throughout the matrix permit the entire microstructure to creep uniformly [7]. Form the histogram tail and the increase in mean value, can be conclude that there is an increase of big particles due diffusion, which could be correlated with Cu_6Sn_5 due is higher diffusivity.

In order to asses a proper identification of particles, an X-Ray map (Figure 21) in the center of sample was accomplished. It shows a spread of Ag_3Sn particles of several dimension and a couple of big Cu_6Sn_5 particles embedded in the Tin matrix.

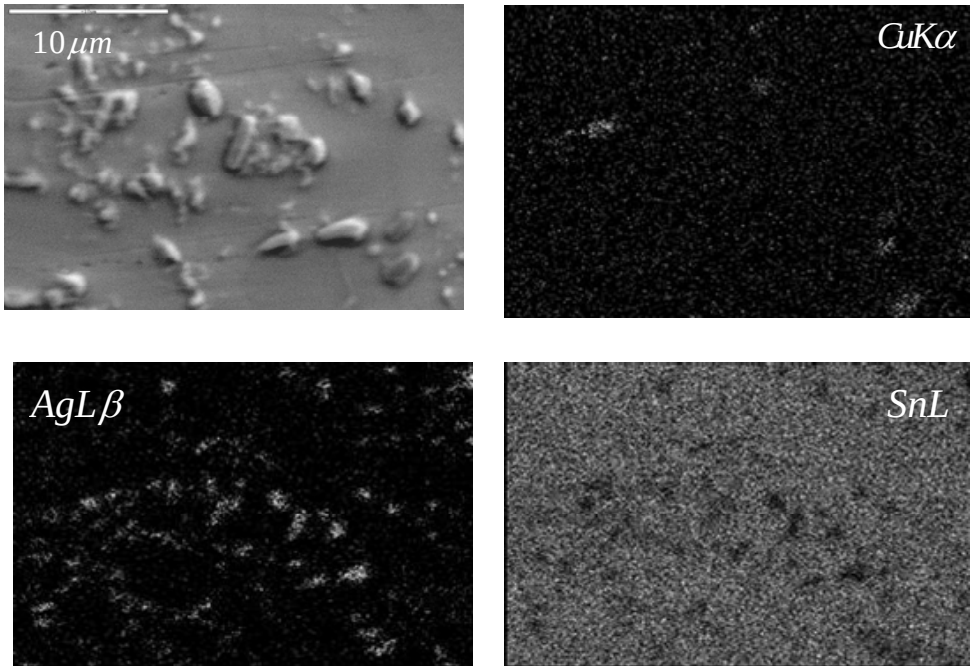

Figure 21. X-Ray map of bulk sample aged 180^{0}C-100h showing Ag_3Sn and Cu_6Sn_5 particles.

From the X-Ray map can also be seen that the Cu_6Sn_5 particles are big and widely spaced to be an effective strengthening mechanism, from which can be concluded that Ag_3Sn particles are the major contributors to creep resistance of the alloy [7,18,22,29].

3. Effect of Aging on Creep Behavior

From Figure 22, it can be seen that the stress exponent (n) calculation for the present work is a little bit under the reported data in literature. This difference is due the highly scatter and variability of data from the experimentation procedure selected. Despite the scatter mentioned, it shows a close enough stress exponent to guess that the creep mechanism is conserved. It also shows clearly a trend that an increase in the operational temperature, in this case, the test temperature, increase the creep rate of the solder.

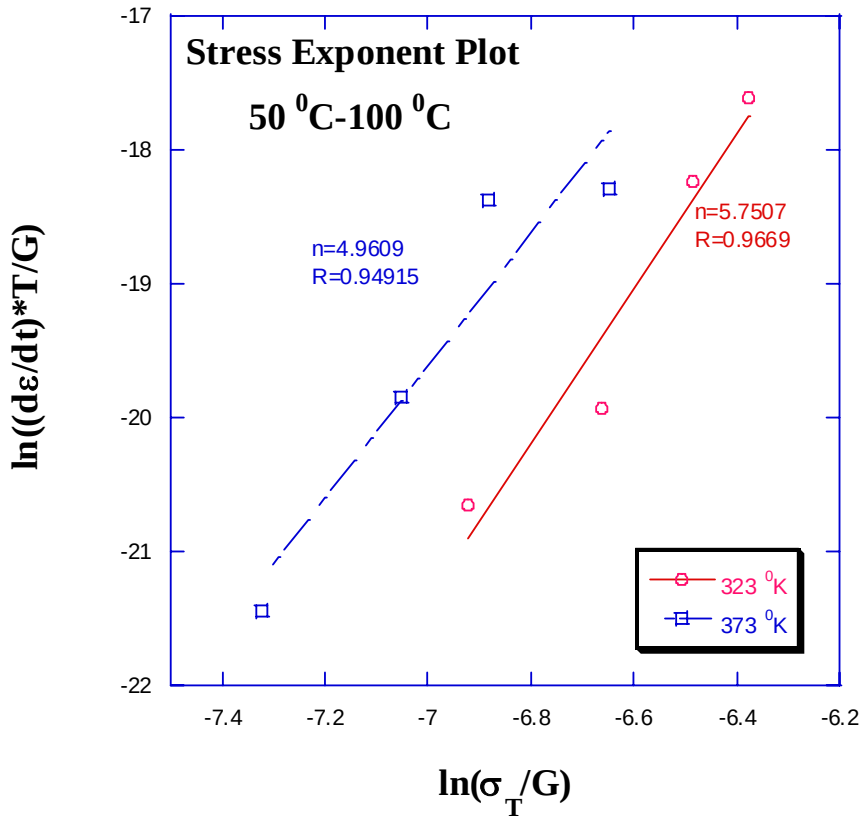

Figure 22. Stress exponent calculation diagram showing increase of creep rate with increasing temperature.

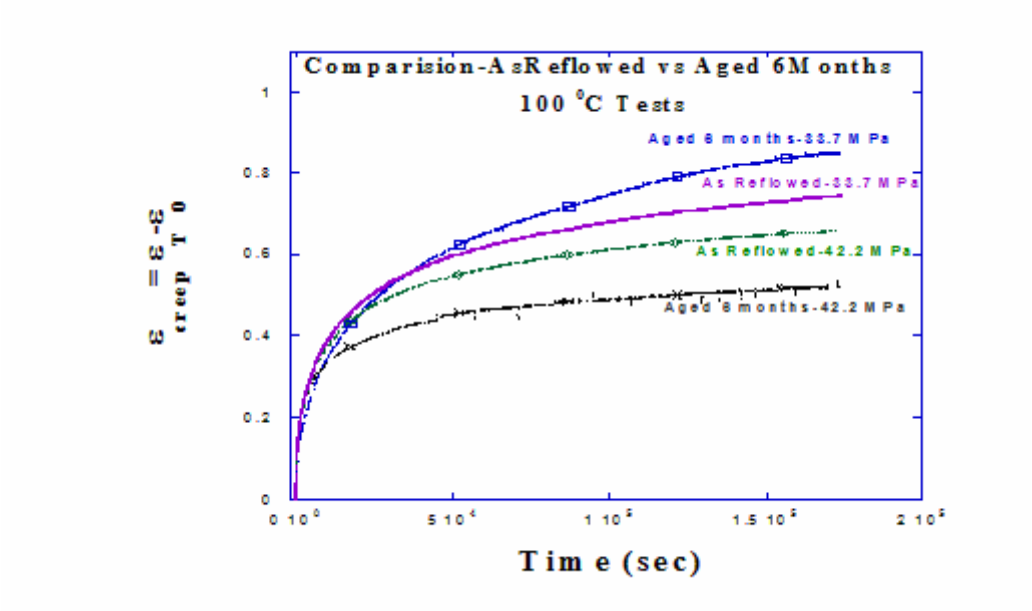

Figure 23. Comparison of as-reflowed vs. aged six months at room temperature creep test.

In order to asses aging effect on the creep behavior, a couple of samples Aged six months at room temperature were tested at 100^{0}C and 48 hours at the same stresses of as-reflowed samples. It can clearly see from Figure 23, that all four samples developed a steep primary strain (first stage) and a steady state (second stage). In order to represents only the creep part, the instantaneous strain (ε_0) was subtracted. The as-reflowed samples show an increased instantaneous strain (ε_0) as stress is increased. The aged sample at 33.7 MPa crept more than the one in an as-reflowed condition. This is because the increase in particle size due aging diminished the creep resistance of solder. The sample aged and tested at 42.2 MPa developed a greater instantaneous strain (ε_0) and finally crept more than the as reflowed sample.

B. STRESS EFFECTS IN MICROSTRUCTURE

As parts of research and after testing several samples, a couple of them were selected in order to asses the effect of stress on microstructure. Therefore, two samples were selected, the highest and lowest stressed samples tested at 100^0C for 48 hours. The samples selected were number 31, tested at 42.2 MPa, and number 32, tested at 11.2 MPa.

A first examination of metallography (Figure 24) for low stress (11.2 MPa), can be noted that the Tin dendrites are clearly seen surrounded by eutectic particulates. From micrograph on Figure 25 shows a very distinguish feature. In one hand shows clearly dendrites surrounded by eutectic particulates, but also a great particulate extent in the lower part. An inspection found that misoriented dendrites colonies collapsed in that area, due the compression test, increasing the local strain. This in turn created an inhomogeneous strains distribution locally but a more homogenous in the rest of sample, where dendrites and eutectic particulates can clearly be seen.

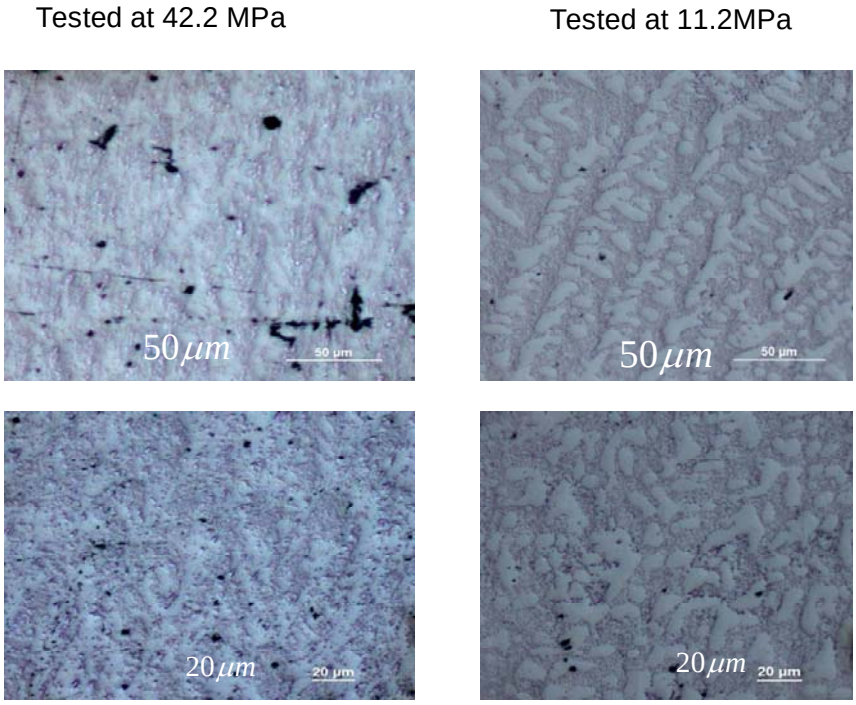

Figure 24. Comparison metallography of 11.2 MPa vs. 42.2 MPa 100^{0}C-48h at high and low magnification.

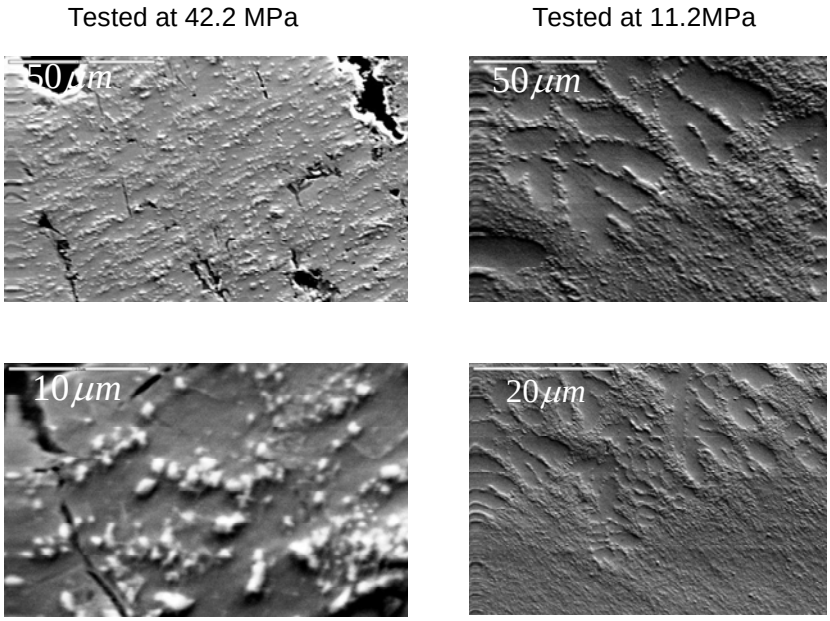

Figure 25. Comparison micrograph of 11.2 MPa vs. 42.2 MPa 100^{0}C-48h at high and low magnification.

An analysis of the metallography (Figure 24) and micrograph (Figure 25) of sample number 31, tested at high stress (42.2 MPa), revealed that the Tin dendrites tend to disappear while particulates tend to coarse and increase spacing amongst them.

From the micrograph in Figure 25, it can be seen that the size and morphology of coarse particulates, resembles that in the sample artificially aged at 180^0C-100 hours (Figure 19). In order to assess this appreciation, the particulates were measured using the same ellipse method and presented in form of a histogram and probability diagram (Figure 26). From histogram was obtained a mean value of 0.91647 μm and a median value of 0.87195 μm. Comparing the histogram for the artificially aged sample (Figure 20) it can be seen that the highly stressed sample has a lower mean value. This means that it has lower amount and size of big particles, but has a higher median value, which correlates well with Ag_3Sn particles. As a result, it can be concluded that Ag_3Sn particles suffered a coarsen effect by volume diffusion but strain-enhancement effect was even greater than diffusion only. This strain coarsening during deformation is attributable to the generation of excess vacancies caused by local hydrostatic stress state and instantaneous inelastic strain rate, therefore augmenting diffusive flux, hence, the coarsening kinetics [17].

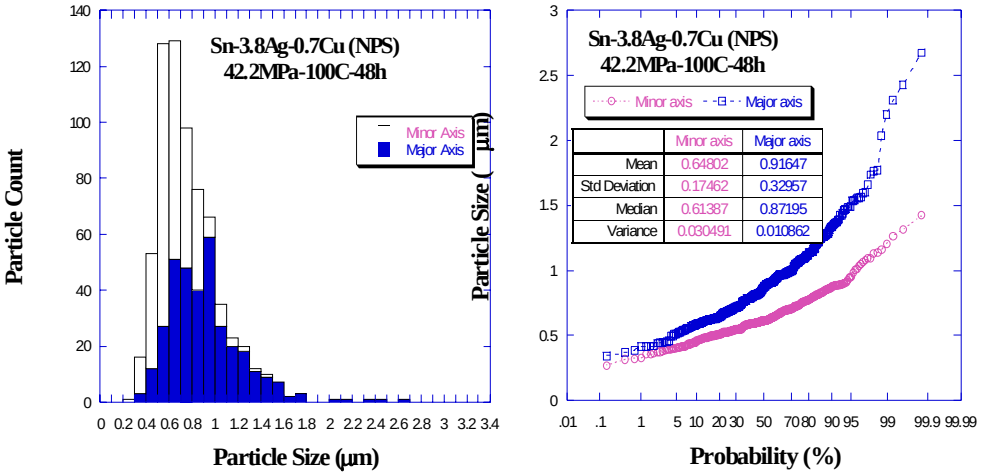

Figure 26. Histogram and Probability Diagram of 42.2 MPa-100^{0}C-48h.

C. AGING EFFECTS IN BALL JOINTS

As a component of SAC-387 research, a few samples were received from *Purdue University.* They were mounted in form of a ball joint of about 650 μm between two plates of silicon, resembling a package assembly. These samples were tested at *Purdue University* under lap shear. The idea was to characterize the microstructure of the samples corresponding to aged 15 days at room temperature and aged 60 days at room temperature (25^{0}C) without having been tested, and compare the results with the bulk samples under testing at Naval Postgraduate School (NPS). In order to accomplish the task, the samples were mounted and polished following the same procedures described in Chapter III.

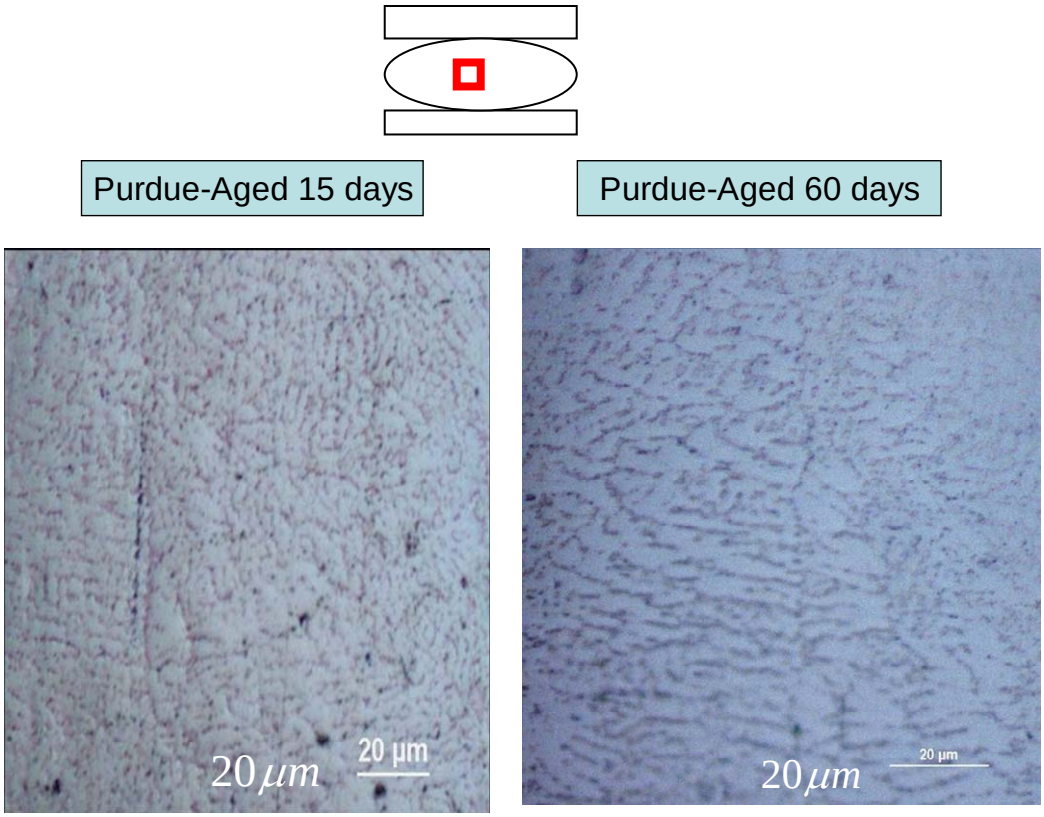

Figure 27. Metallography of *Purdue* samples showing eutectic particles.

The observation of optical metallography (Figure 27) indicates a Sn matrix with discontinuous eutectic particles around them. The previous observation is supported by SEM Micrographs (Figure 28) for a 15 days aging at room temperature. However, it is noted that for aged 60 days there is an increase in particles coarsening in a Tin matrix.

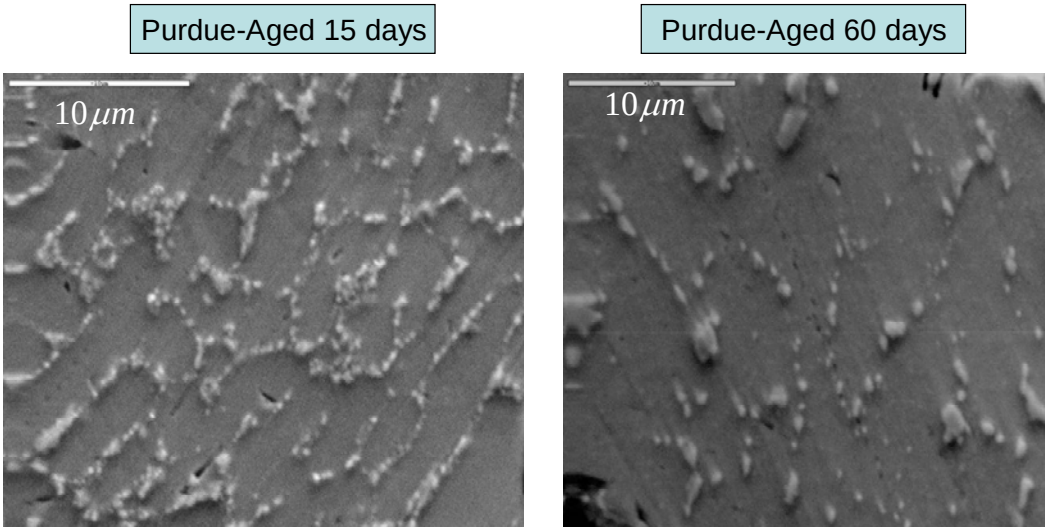

Figure 28. Micrographs of *Purdue* ball joints at high magnification showing difference in particles.

Considering that the increase of particle size is notable for a natural sample aged 60 days at room temperature when compared with a bulk sample aged six months at room temperature as well, a measurement of particles was accomplished and results presented in form of a histogram (Figure 29). From the histograms can be obtained a mean value of 0.50857 μm and median of 0.45397 μm in major axis for aged 15 days; a mean value of 0.79076 μm and median of 0.67500 μm for major axis for aged 60 days sample.

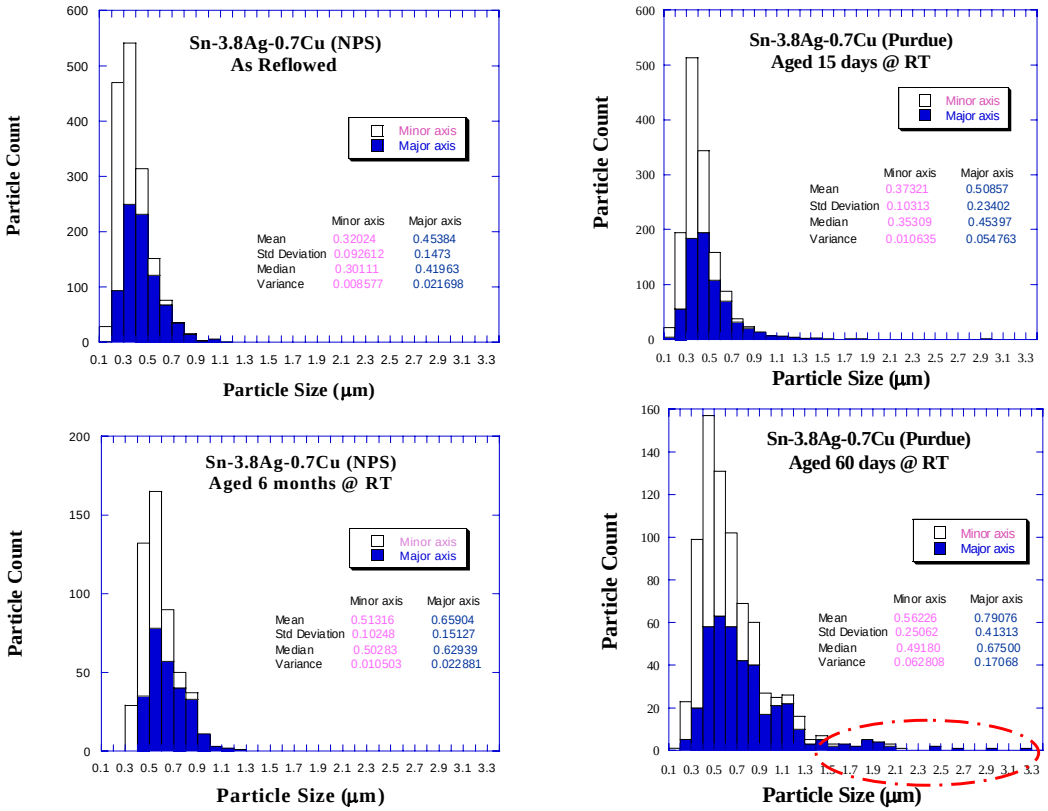

Figure 29. Comparison histograms of *Purdue* vs. NPS samples.

Considering that the bulk samples from NPS and the Purdue samples are exactly the same solder composition (SAC-387), a correlation in the aging effects for both of them is expected. Comparing the histograms for as-reflowed, aged six months at room temperature and histograms for both *Purdue* samples, we can see that for bulk samples (NPS) there was a 45.2% increase in mean and 50% increase in median values. For *Purdue* samples the increase was 55.5% in mean and 48.7% for median values. These values indicate that there is an increase in big particles number (mean value) compared with bulk samples; and the Ag_3Sn particles for both kind of samples are comparable in size increasing (median value).

A feature that caught attention is the fact that the aged 60 days *Purdue* sample developed a prominent tail in the histogram. It can be seen that a 100% increase in big particles count, as highlighted in Figure 29, presents a question that needs to be addressed.

The Ball Joints were manufactured in *Texas Instruments* for *Purdue University*. They were mounted in Tungsten Bond Pads with an Electrolytic Nickel-Gold (ENIG) coating. Therefore, and considering the Phase Diagrams, the big particles are likely to be Ni_3Sn_4 and/or Au_3Sn. That information drives the search for a proper explanation for the histogram tail of *Purdue* aged 60 days sample (Figure 29).

Purdue-Aged 60 days

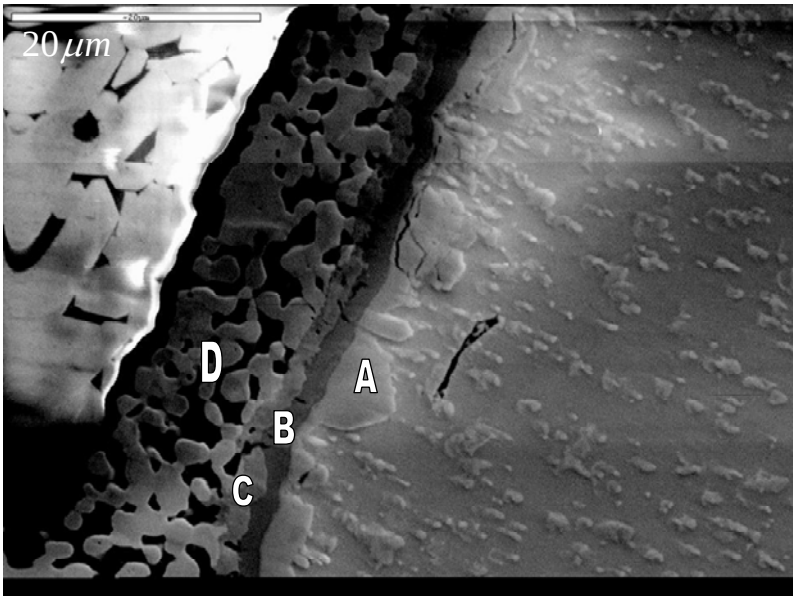

Figure 30. Purdue aged 60 days at room temperature showing left interface.

Purdue-Aged 60 days

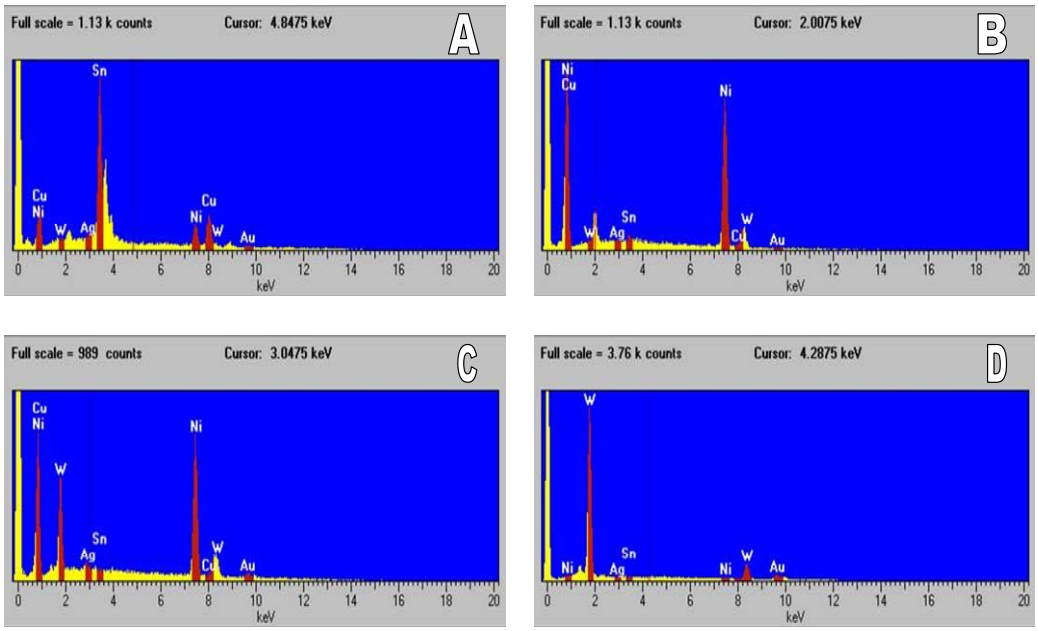

Figure 31. X-ray map at left interface of aged 60 days at room temperature ball joint.

From the micrograph (Figure 30) can be seen scallops coming from the interface, but also several layers of very distinct colors. The X-Ray point analysis (Figure 31) shows point D as Tungsten, which corresponds clearly to the Bond Pad. For a light gray layer at point C it shows a combination of Tungsten, Nickel and Copper. It is worthy to note that the Cu and Ni peak are at the same peak. Since the Energy Resolution of *SEM TOPCON SM-510* is 0.133 KeV, it is not possible for the EDX to resolve between $NiL\alpha$ (0.8515 KeV) and $CuL\alpha$ (0.9297 KeV). Knowing that the pad bond is coated with Nickel, the Cu peak was disregarded. However, a close look at the W-Ni phase diagram shows that about 40% W,

Ni comes in solid solution with W, which gives a reasonable explanation for the W and Ni peaks at that point. The analysis of Point B shows mostly Nickel and some Gold, and can be correlated clearly with Ni coating. However, for point A, the scallop shows Nickel, Tin, Copper ($K\alpha$), Silver and some Gold. In order to resolve this further investigation of the area was needed.

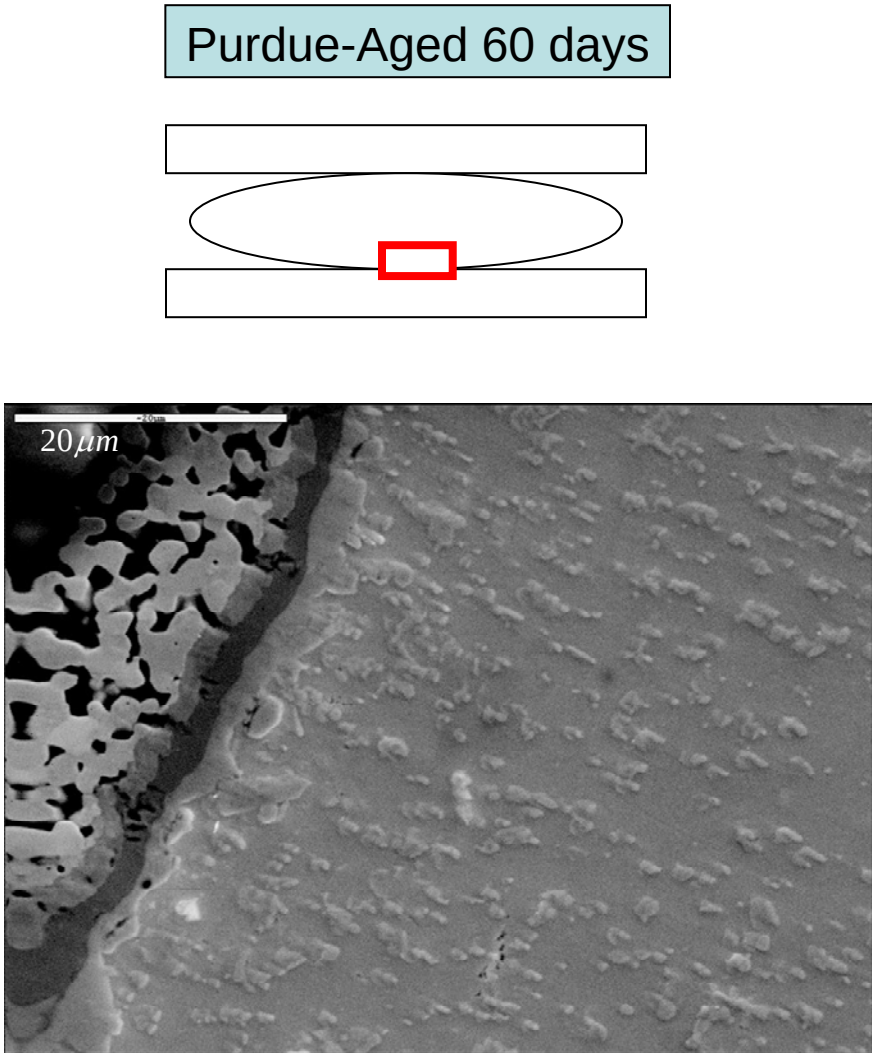

Figure 32. Purdue aged 60 days - Scheme and left interface.

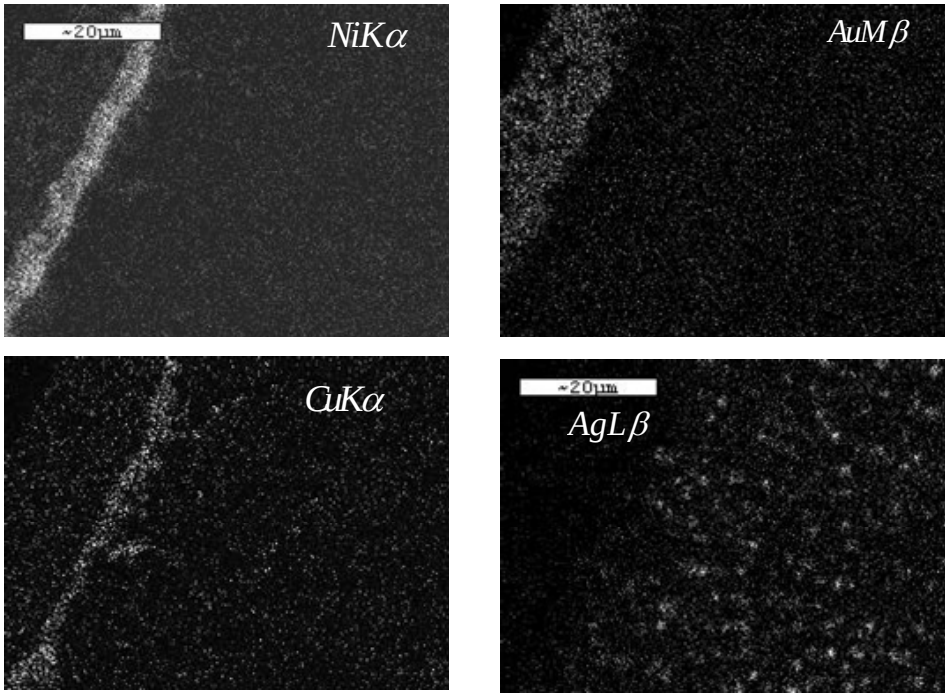

Figure 33. X-Ray map of aged 60 days showing evidence of Ni and Cu reaction at left interface.

Further investigation of the left interface (Figure 32 and 33) with the aid of X-ray map was accomplished in the area of study. Despite de Tungsten and Tin (not showed), there is a big amount of Ag_3Sn particles in the adjacent zone of the interface. Gold was also founded and correspond a Gold atoms from the coating and a small amount that are reacting with Sn to form Au_3Sn. For Nickel, from coating also, there is evidence of intermetallic reaction at interface. However, it was found a rich Copper area at scallops, which is also reacting at the interface. A close look at the Ni and Cu map shows that the same particles correlate with Ni and Cu, creating ternary eutectic in the zone adjacent to the left interface.

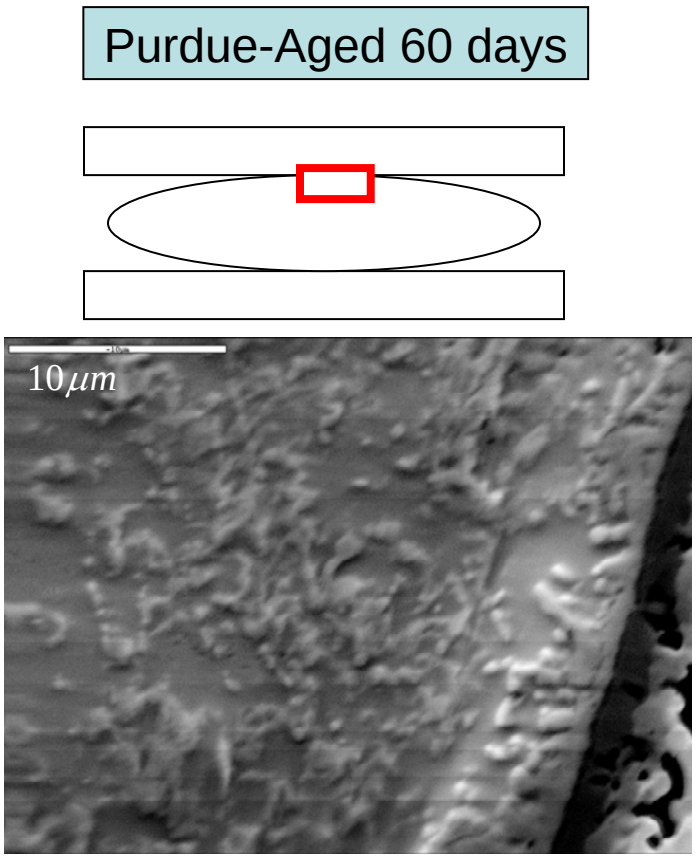

Figure 34. Purdue aged 60 days - Scheme and right interface.

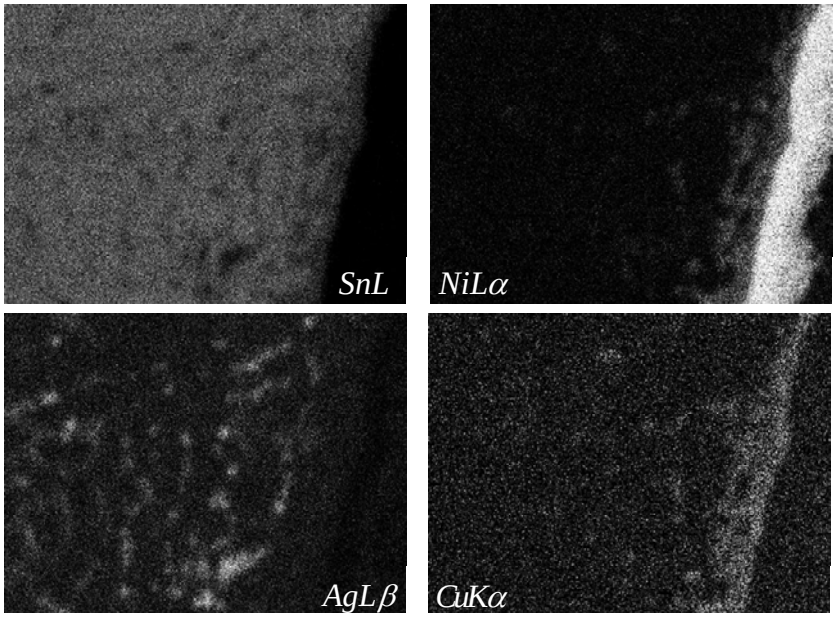

Figure 35. X-Ray map of aged 60 days showing evidence of Ni and Cu reaction at right interface.

It is noteworthy that the right interface shows a big amount of scallops and chunky and irregular particulates. It is noteworthy to establish also, that the Ni and Cu correlate clearly on the same particulates on this interface. This is evidence of ternary reaction among Cu and Ni with Sn to form an intermetallic as stated before. This is due a complete solubility (isomorphous system) of Ni and Cu, where Ni substitutes Cu in the Cu sublattice [17].

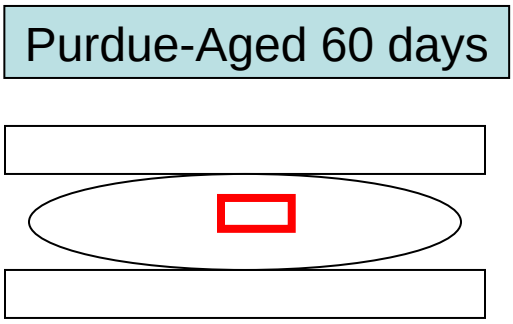

Figure 36. Scheme of a *Purdue* ball joint.

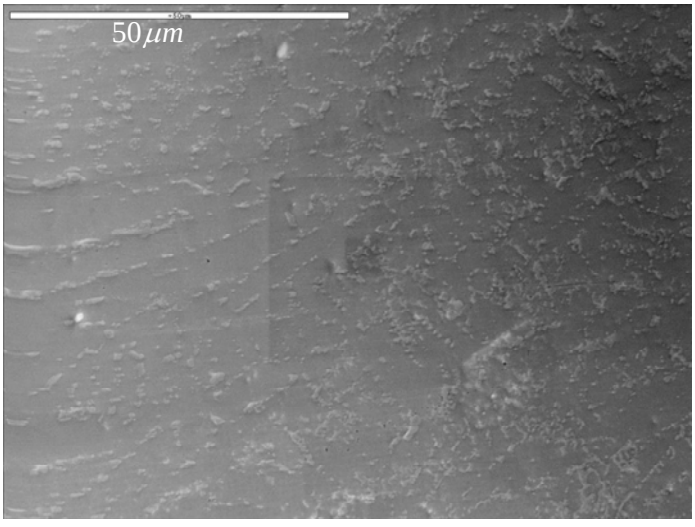

Figure 37. Purdue aged 60 days- micrograph at center ball joint.

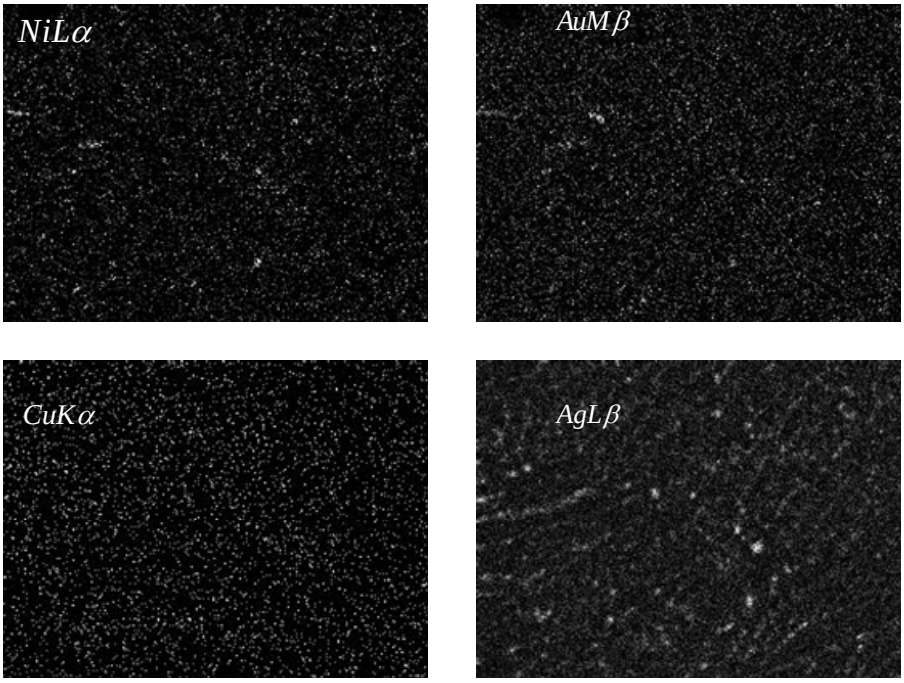

Figure 38. X-Ray map at center of *Purdue* aged 60 days showing depletion of Cu.

In order to assess the distance diffused by Ni and Au atoms into the ball joint, an X-ray map was accomplished at the center of the ball joint. It shows evidence of Ni_3Sn_4 and Au_3Sn particles in the center but spread out and in small amount to explain by itself the abnormal increase of particles size for Ball Joints compare with Bulk Samples. Is noteworthy the almost absence of evidence of Cu at the center, but clearly appears at interfaces.

Zribi et al., [34], Ho et al., [35] stated that in the presence of Cu, the Ni_3Sn_4 particles did not grow at the interfaces. For the composition of SAC-387, and due the depletion of Cu in the center of the ball, is expected the growth of a ternary named $(Cu,Ni)_6Sn_5$, because Ni atoms substitute for Cu atoms in the sublattice of Cu. This

ternary growth at the interface and can be seen by the correlation of Ni and Cu X-ray maps at both interfaces.

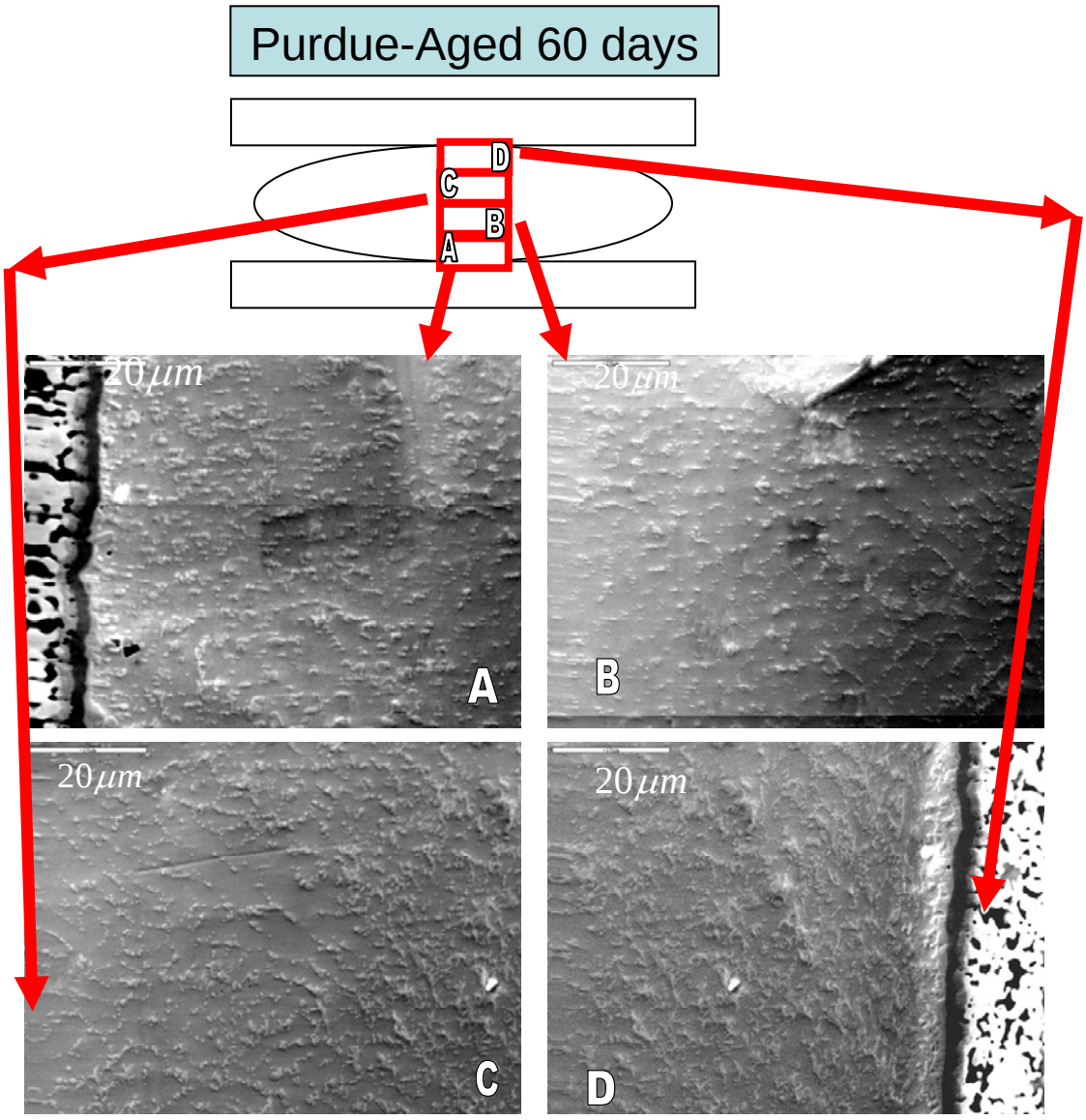

Figure 39. Panoramic view of Purdue aged 60 days showing difference in microstructure along interfaces.

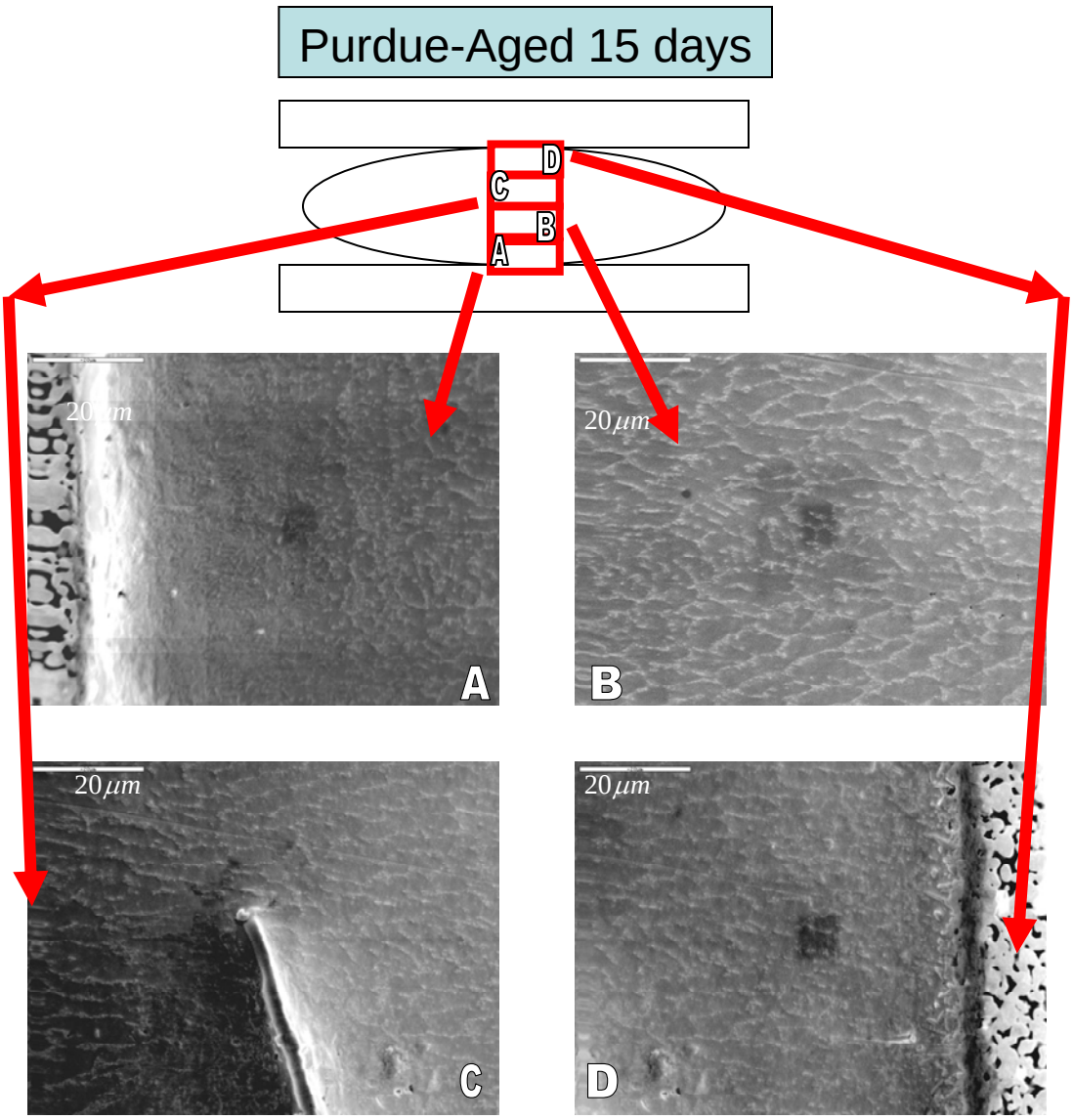

Figure 40. Panoramic view of Purdue aged 15 days showing consistent microstructure.

Considering the differences seen in both samples, a panoramic view across the entire ball joint was accomplished. It reveals that for 15 days sample (Figure 40) the microstructure is much more uniform across the ball, revealing the discontinuous eutectic particles. On the other hand, for 60 days sample (Figure 39), there is big change in

microstructure across it. The left interface shows a little bit coarsen particles than in the center, but coming into the right interface, the particles show a bulky and irregular form.

As a conclusion, the increase in particles size for ball joints aged 60 days at room temperature is due to several effects. On the one hand is the evidence of Ni and Cu reacting to form a ternary intermetallic compound. However, the ternary reaction is occurring mainly at the interfaces, which presents bulky and irregular particles, especially at the right interface. Evidence was also found of Ni and Au particles forming a binary intermetallic compound at the center, which increase the amount and size of particles counted. However, the particles found were in majority Ag_3Sn, which experienced an increase in coarsening kinetics. Considering what stated by Dutta [12] in equation 25 of his paper, the particle size is a function of the molar volume of the second phase (V_M), equilibrium solute concentration in the matrix (C_0), the specific energy of particle-matrix interface (γ_S), effective solute diffusivity in the matrix (D_{sol})and time (t), it is believe that the depletion of Cu in the solder matrix, leaving a almost binary composition, alter the equilibrium solute in the matrix, enhancing the growing kinetics of Ag_3Sn.

Is worth noting that the micrographs used to measure particles (Figure 29) came from center-right side of the 60 days sample (area C in Figure 39).

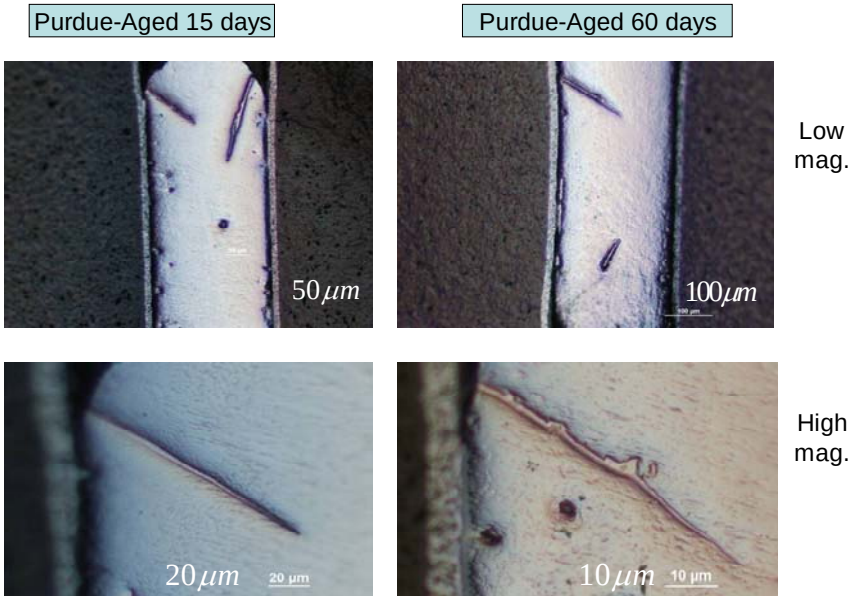

Figure 41. Metallography of *PURDUE* samples.

Another feature that caught attention at first look at the metallography of both aged samples is the appearance, after polishing, of the needles depicted in Figure 41 in almost on the same position for both samples. It is noteworthy that the needle for 15 days sample looks sharp and clean, whereas the 60 days sample have scallops attached.

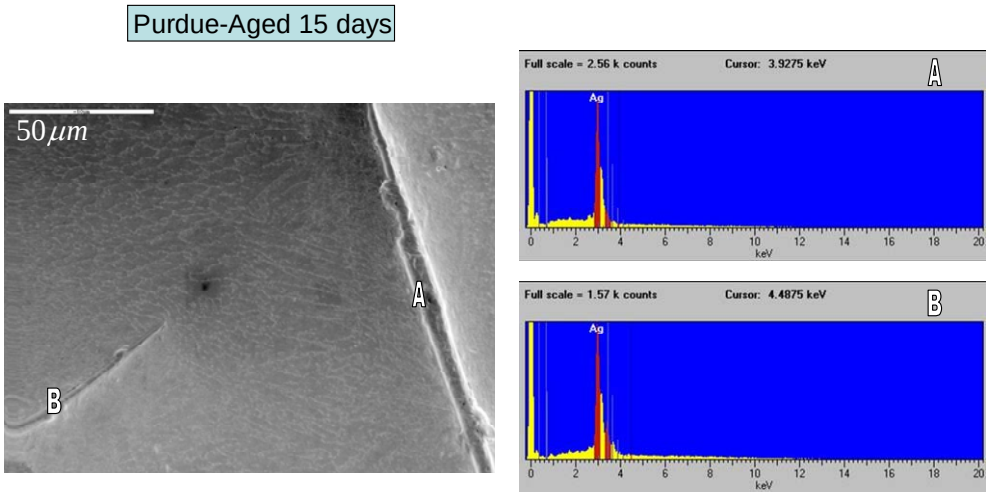

Figure 42. Point X-Ray Analysis of 15 days sample needles.

A first attempt to identify the needles composition was made in the 15 days sample with the aid of a point x-ray analysis, which shows clearly Ag and Sn, being identified with the aid of the phase diagrams as stoichometric Ag_3Sn. Kang et al., [15] amongst other authors have reported the formation of this big Ag_3Sn needles during solidification at moderate to slow cooling rate, where the pro-eutectic phases of Ag_3Sn can grow to large sizes within an undercooled liquid before nucleation of the $\beta - Sn$ phase and before the final solidification of the ternary interdendritic microstructure. The presence of Cu, also, promotes the formation of large Ag_3Sn needles at early stages of solidification, possibly by assisting the nucleation of the plates [15].

However, the growth of large pro-eutectic phases can be reduced kinetically by a rapid undercooling and thermodynamically by reducing Ag or Cu content. [15]

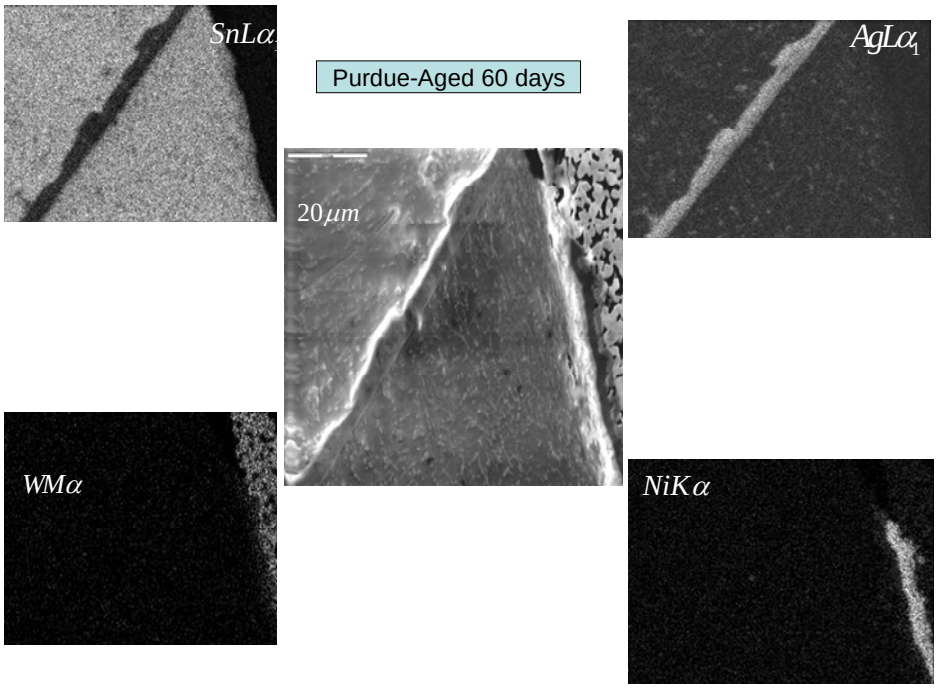

Figure 43. X-Ray map of aged 60 days – Needle.

The needle in the aged 60 days sample was also investigated with the aid of an X-ray map (Figure 43) of the area, showing clearly that the needle composition is Ag_3Sn. Since this was done very close to the interface, the map also shows the Tungsten Bond Pad and Nickel, the latter showing some scallops as stated before.

D. CURVE FITTING

The response of a body to an applied stress elastic, anelastic, and plastic generally depends on stress magnitude, strain rate ($d\varepsilon/dt$), temperature, and structure. An elastic deformation takes place at the instant of stress application and disappears at the instant of stress removal. Since the elastic strain is reversible and time independent, its magnitude is a single valued function of stress.

Anelastic deformation depends on deformation rate and structure, being also reversible but time dependent. On the other hand, plastic deformation is irreversible, imposing a permanent change in the body, being a compound of time dependent and time independent components. The time dependent component of plastic deformation is designated as creep. [32]

When stress is applied at the beginning of the creep test, the initial strain rate is immeasurable fast, being more convenient to define an initial strain (ε_0) rather than a strain rate on loading. These initial rapid deformation strains harden the material, allowing to the measuring of the subsequent change in strain with time [33]. A normal creep curve will show three stages: a primary part or first stage, where rate of hardening is greater than rate of softening (relaxation); a secondary stage or steady state, where rate of hardening is equal to the rate of softening (relaxation); and a tertiary stage, where the rate of hardening is much less than the rate of softening, showing commencement of necking and leading to fracture of materials under tension test.

Considering that for the present work the testing procedure selected was a compression test under constant load, the creep curves exhibit a fast primary creep achieving a secondary stage, or steady state, but does not exhibit tertiary stage. The calculated creep curves after testing are displayed as Figures 9, 10, and 11.

Hence, considering that at any time during creep test the total strain can be expressed as:

$$\varepsilon_{Total} = \varepsilon_0 + \varepsilon_C$$

where ε_0 is the initial or time-independent strain and ε_C is the time-dependent or creep strain. Therefore, total strain can be also expressed as:

$$\varepsilon_{Total} = \varepsilon_0 + \varepsilon_{pri} + \varepsilon_{ss} = \varepsilon_0 + \varepsilon_{pri} + \frac{d\varepsilon_{ss}}{dt} * t$$

where ε_{pri} is the primary strain; ε_{ss} is the steady state strain, which can be also expressed as steady state strain rate ($\frac{d\varepsilon_{ss}}{dt}$) plus the elapsed time (t) for the creep test. From the curves (Figures 9, 10, 11) were obtained the initial strain (ε_0), steady state strain rate ($d\varepsilon/dt$) and the total strain. Therefore, after algebraically arranging the equation above, the primary strain was captured and depicted in Figures 44, 45 and 46. Is worth noting that for 15 MPa – 150^0C – 48 h test, depicted in Figure 43, the strain rate was still increases. Since the primary creep does not reach a steady state it is believed that the test is not reliable, hence, the data for 150^0C tests was discarded.

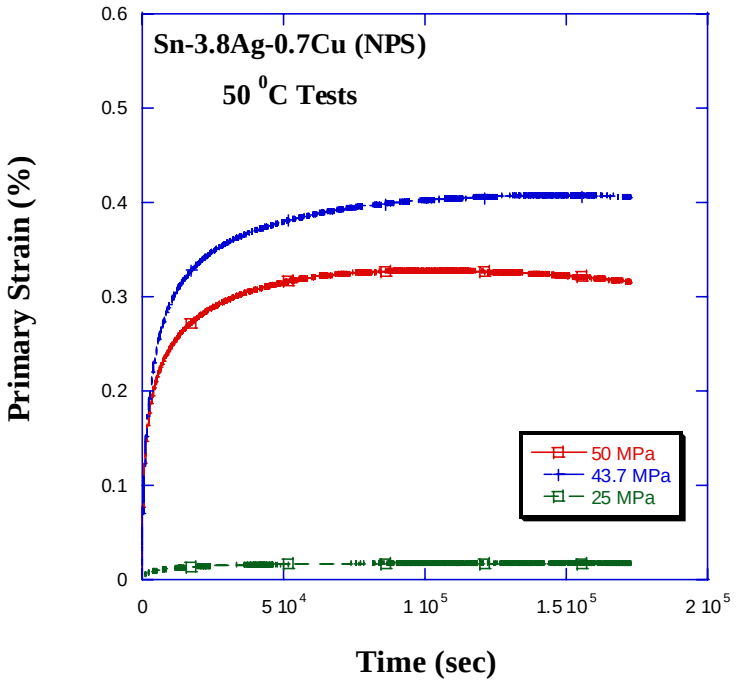

Figure 44. Primary creep diagram at 50^{0}C.

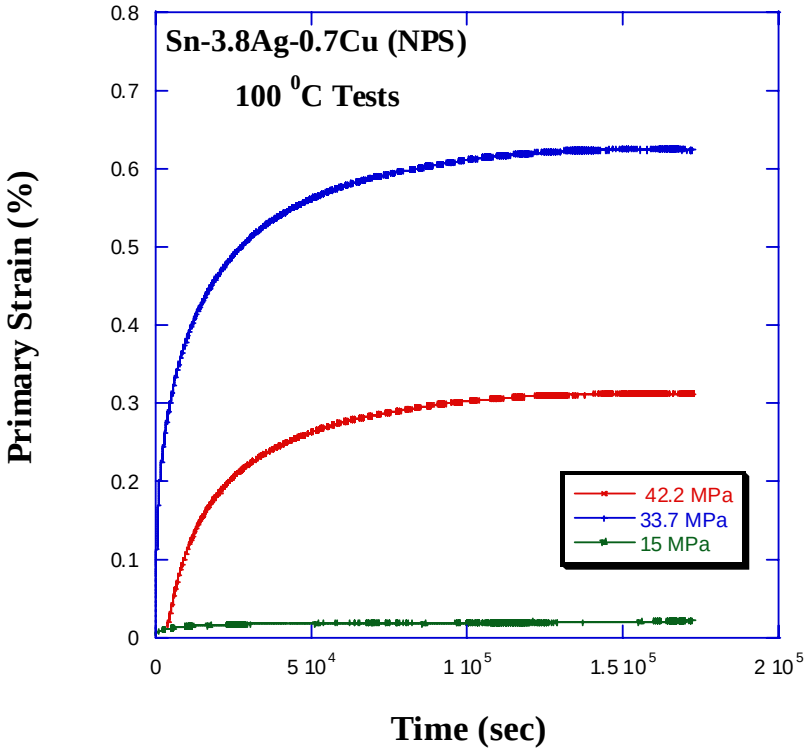

Figure 45. Primary creep diagram at 100^{0}C.

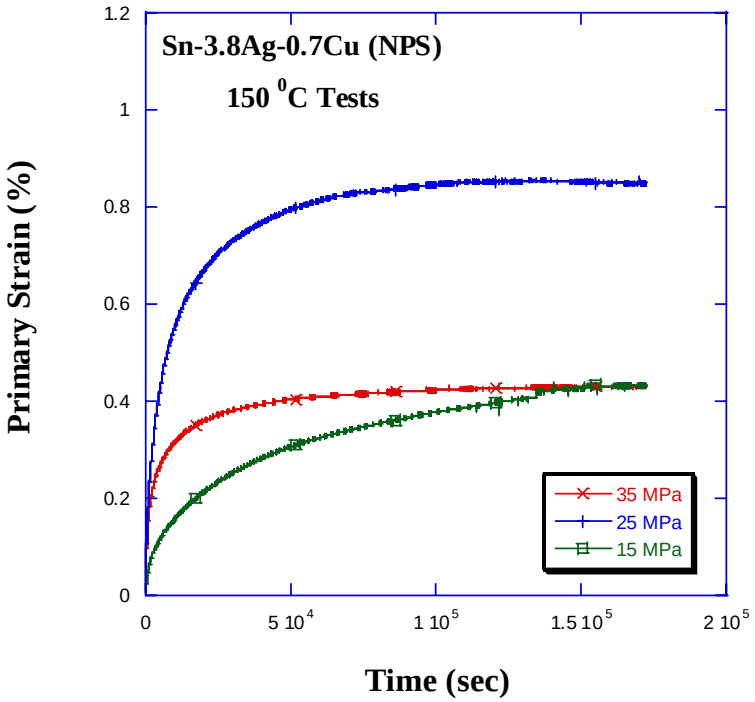

Figure 46. Primary creep diagram at 150^{0}C.

The graphical representation of the primary creep curve is adequate when tests are performed to establish how certain parameters vary with stress and temperature for the solder. However, for practical and theoretical purposes, it is often desirable to devise equations which can describe the rate of strain accumulation with time [33]. The idea is replaced this graphical representation by an analytical procedure which permits to represent the curve in terms of a set of parameters, where the values of the coefficients allows to specified the curve in terms of strain and time of equation used.

Studies of the creep behavior of single crystal of zinc suggested that the strain/time curve could be well represented by a modified Andrade equation having a form of [33]:

$$\varepsilon_c = at^{1/3} + ct$$

However, for several materials, a single term of $t^{1/3}$ has been found to be inadequate to described primary creep curves. Therefore, a third degree polynomial is recommended having a form of [33]:

$$\varepsilon_c = at^{1/3} + bt^{2/3} + ct$$

As an alternative, it was found that a representation of curve shape is better captured by a term $t^{1/2}$, proposing an equation having the form of:

$$\varepsilon_c = at^b + ct$$

with parameter b varies from zero to unity. However, the major disadvantage of this proposed formula is the strain rate representation:

$$\frac{d\varepsilon}{dt} = abt^{(b-1)} + c$$

Considering that b varies from zero to unity, the formula predicts at $t \rightarrow 0$ a strain rate $\frac{d\varepsilon}{dt} \rightarrow \infty$. The prediction of an infinite creep rate makes the proposed equation unsuitable for this work. For this reason it was disregarded.

An equation proposed by Evans & Wilshire [33] that eliminates the objections of the first equation at $t \rightarrow 0$ is more adequate to represents the creep of materials having the form of:

$$\varepsilon_c = a(1 - e^{(-bt)}) + ct$$

where the creep rate at any time for the equation above is going to be having a form of:

$$\frac{d\varepsilon}{dt} = abe^{-bt} + c$$

where **a** is the total primary creep strain; **b** determines the rate of exhaustion of the primary stage; and **c** closely approaches to the steady state strain rate ($\frac{d\varepsilon}{dt}$).

Therefore, the equation of total strain must have the form of:

$$\varepsilon_{total} = \varepsilon_0 + \varepsilon_{pri} + \varepsilon_{ss} = \varepsilon_0 + a(1 - e^{-bt}) + ct$$

This equation was selected to described and fitted, with the aid of *Kaleidagraph 3.5*, to the primary curves (Figures 44, 45, 46). However, there is a high variability in results, which makes it difficult to understand the physical meaning of the coefficients obtained, therefore no further analysis was made.

Considering the data supplied by Professor Subbarayan from *Purdue University,* a preliminary analysis was made. The samples were tested in lap shear at 25^0C, 75^0C and 125^0C, been Time and Strain recorded for analysis purposes. In Figure 47 is depicted the Strain versus Time for test accomplished at 25^0C, as an example. It can be seen, that the curves depicted show three stages of a creep curve until fracture.

From the curves were obtained the instantaneous strain (ε_0) and the steady state strain rate ($d\varepsilon/dt$) and by the use of equation depicted below the primary creep was captured.

$$\varepsilon_{Total} = \varepsilon_0 + \varepsilon_{pri} + \varepsilon_{ss} = \varepsilon_0 + \varepsilon_{pri} + \frac{d\varepsilon_{ss}}{dt} * t$$

Once the primary creep was isolated with the aid of *Kaleidagraph 3.5* and the equation proposed by Evans & Wilshire was fitted. The fitted curves can be seen in Appendix A.

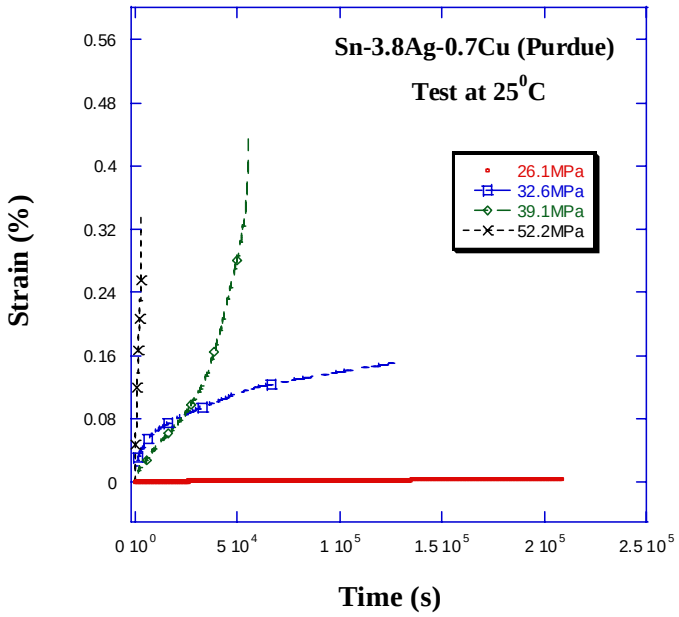

Figure 47. Purdue test example at 25⁰C.

It is believed that **c** is close to the steady state creep rate and it is assumed to be exponentially related to **a** and **b** coefficients obtained from the curve fitting. The relation is depicted in the form of:

$$c^A \approx \frac{ab}{kB}$$

$$\ln\left(\frac{ab}{k}\right) = \ln\left(c^A\right) + \ln B$$

where the coefficients A and B are constant which can be determined by using a log-log fitting curve.

Purdue-25^{0}C					
Stress (Mpa)	a	b	SS Strn Rate ©	A	B
26.1	0.001195	3.72E-05	1.23E-08		
32.6	0.046436	0.002498	1.05E-06	0.9003	1.081231
52.2	0.079535	0.001292	6.54E-05		

Table 4. Summary for curve fitting at 25^{0}C.

Purdue-75^{0}C					
Stress (Mpa)	a	b	SS Strn Rate ©	A	B
26.1	0.008376	0.00978	2.61E-06		
32.6	0.13808	0.001142	2.59E-05	1.0451	31.77246
39.1	0.071066	0.012471	2.23E-04		

Table 5. Summary for curve fitting at 75^{0}C.

Purdue-125^{0}C					
Stress (Mpa)	a	b	SS Strn Rate ©	A	B
13.04	0.015725	7.85E-05	4.00E-07		
26.1	0.21036	0.004317	1.60E-04	0.914	1.208403
39.1	0.047285	0.25348	1.07E-02		

Table 6. Summary for curve fitting at 125^{0}C.

As a summary from the curve fitting are the results depicted in Tables 4, 5, and 6, where the value for **a** and **b** are shown. Considering a log-log fitting, in order to asses the values of A and B, A comes close to unity. For the case of B, it is less conclusive due to a high variability, however it can be guessed close to unity also.

V. SUMMARY

In this study, the effects of natural and artificial aging were investigated and compared against an as-reflowed sample. The major effect was an increase in mean and median values of the precipitate size, where the median value allows the tracking of Ag_3Sn particles. It has been shown that the increase in the computed particle size is primary due to coarsening of Ag_3Sn particles, although coarsening of Cu_6Sn_5 particles also influences the measurements.

Since the creep resistance is due to the dispersed eutectic particles in the regions are Ag_3Sn, the volume fraction of which is significant higher, is the major contributor of creep resistance of the solder. Aging, due diffusion-controlled mechanism, increases size and spacing of particles, having a detrimental effect on creep behavior. However, the initial particle size, due initial reflowing, is a key issue on the creep behavior.

A couple of samples, at low and high stress, both tested at 100^0C – 48 hours were characterized. It was observed that the particle size in the sample that experienced the higher stress is coarser. This suggest that even with isothermal aging, coarsening is strain-enhanced.

A couple of ball joint samples in two different natural aging conditions were also characterized. One contributor to the increase in particle size is the reaction of Cu and Ni at the interfaces creating a ternary eutectic. It is believed that the depletion of Cu content within the solder ball increases the equilibrium solubility of Ag in Sn, and results in an increased kinetics of Ag_3Sn particles.

Finally, it was demonstrated that the primary creep data for ball joints can be fitted well to exponential law. Fit parameters for the tests accomplished at 25^0C, 75^0C, and 125^0C on ball joints were obtained.

Further studies are recommended for different aging conditions of SAC-387 in order to validate the coefficients given. That will provide a mathematical equation to link particles size and creep. It is also necessary to continue characterizing ball joint following several aging treatments in order to address the role played by Cu in the coarsening of Ag_3Sn particles.

APPENDIX

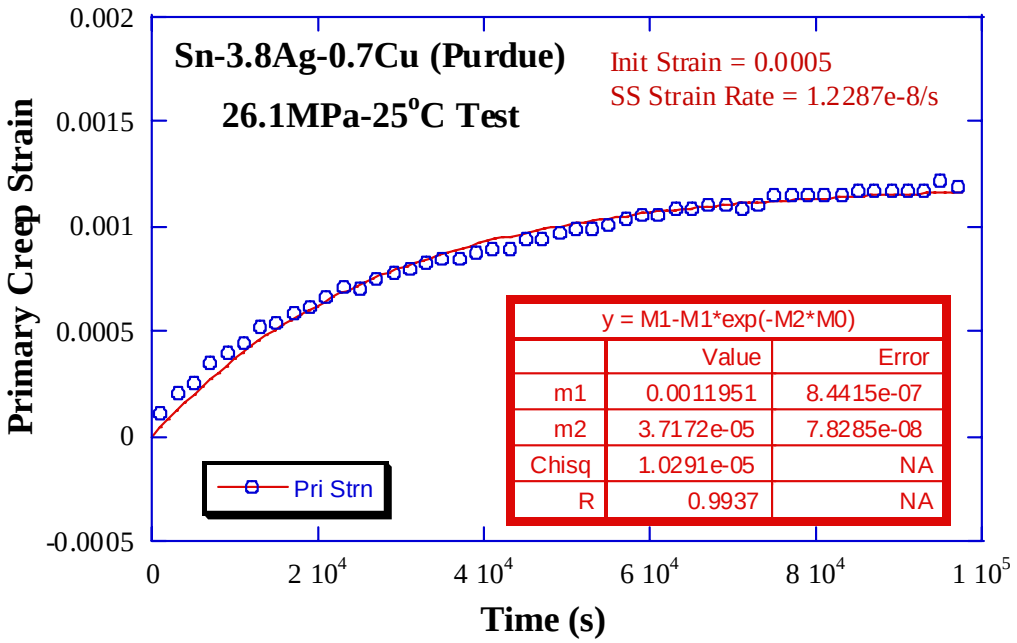
Sn-3.8Ag-0.7Cu (Purdue)
26.1MPa-25°C Test
Init Strain = 0.0005
SS Strain Rate = 1.2287e-8/s
Primary Creep Strain
Time (s)
Pri Strn
y = M1-M1*exp(-M2*M0)
Value Error
m1 0.0011951 8.4415e-07
m2 3.7172e-05 7.8285e-08
Chisq 1.0291e-05 NA
R 0.9937 NA

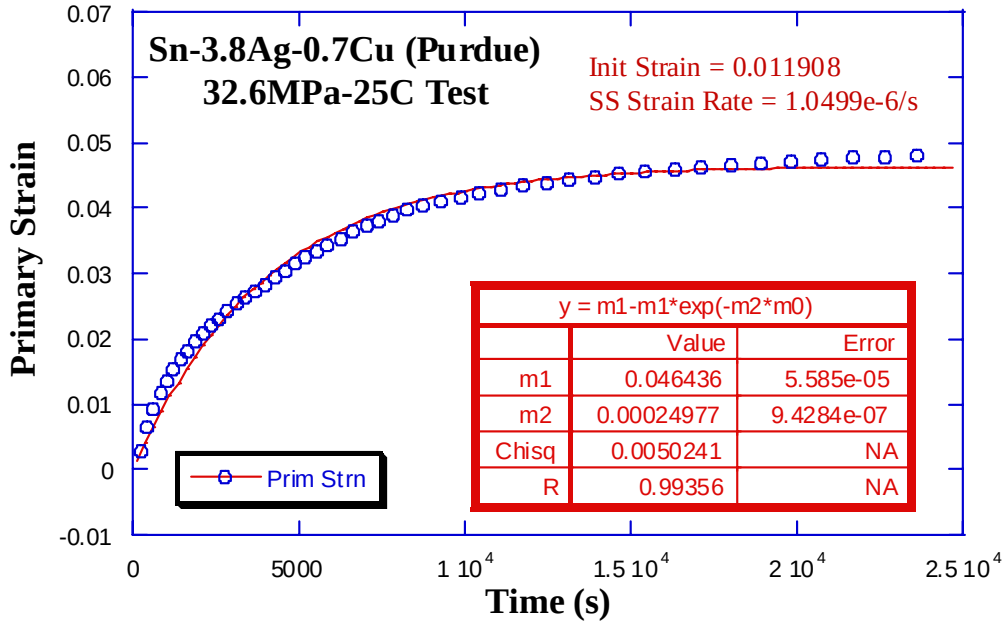
Sn-3.8Ag-0.7Cu (Purdue)
32.6MPa-25C Test
Init Strain = 0.011908
SS Strain Rate = 1.0499e-6/s
Primary Strain
Time (s)
Prim Strn
y = m1-m1*exp(-m2*m0)
Value Error
m1 0.046436 5.585e-05
m2 0.00024977 9.4284e-07
Chisq 0.0050241 NA
R 0.99356 NA

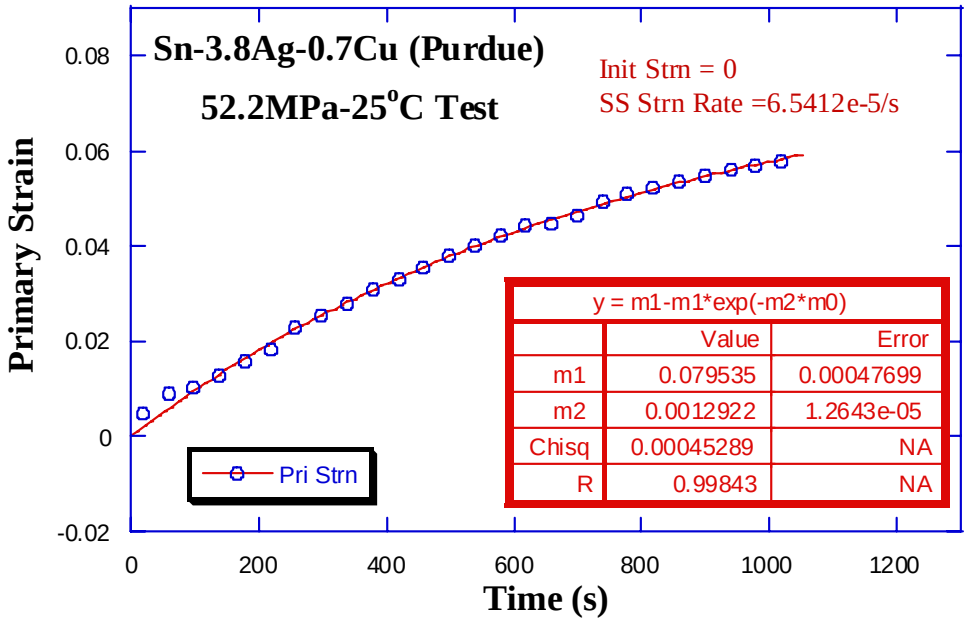
Sn-3.8Ag-0.7Cu (Purdue)
52.2MPa-25°C Test
Init Strn = 0
SS Strn Rate =6.5412e-5/s
Primary Strain
Time (s)
Pri Strn
y = m1-m1*exp(-m2*m0)
Value Error
m1 0.079535 0.00047699
m2 0.0012922 1.2643e-05
Chisq 0.00045289 NA
R 0.99843 NA

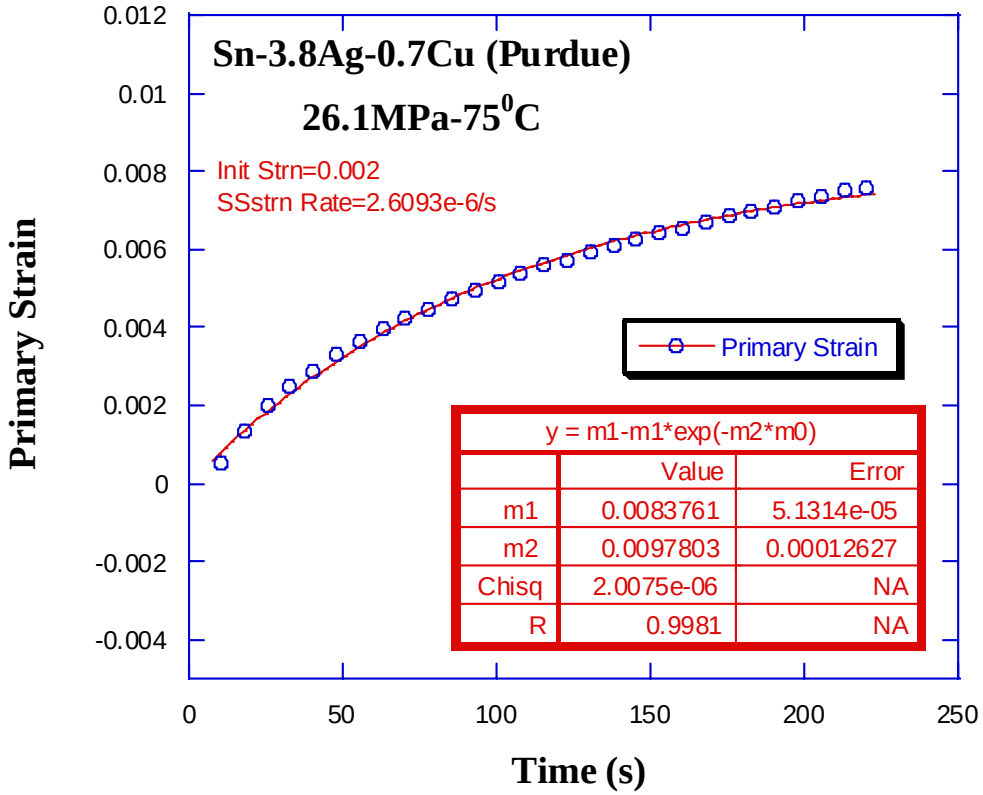
Sn-3.8Ag-0.7Cu (Purdue)
26.1MPa-75°C
Init Strn=0.002
SSstrn Rate=2.6093e-6/s
Primary Strain
Time (s)
Primary Strain
y = m1-m1*exp(-m2*m0)
Value Error
m1 0.0083761 5.1314e-05
m2 0.0097803 0.00012627
Chisq 2.0075e-06 NA
R 0.9981 NA

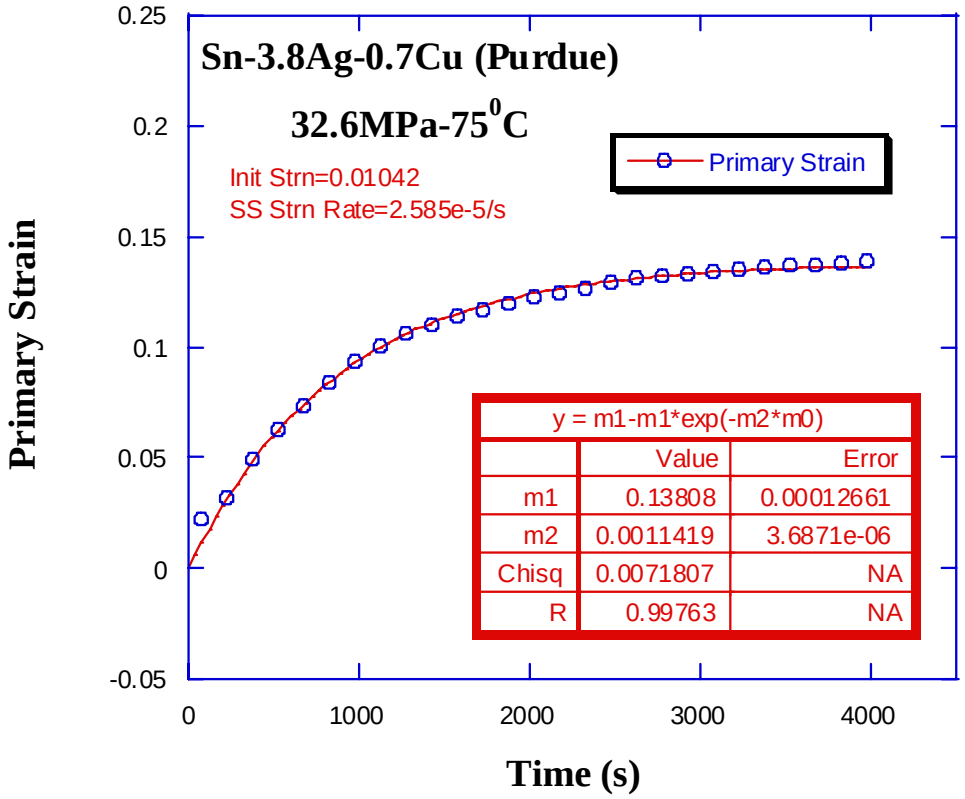
Sn-3.8Ag-0.7Cu (Purdue)
32.6MPa-75^{0}C
Init Strn=0.01042
SS Strn Rate=2.585e-5/s
Primary Strain
y = m1-m1*exp(-m2*m0)
Value Error
m1 0.13808 0.00012661
m2 0.0011419 3.6871e-06
Chisq 0.0071807 NA
R 0.99763 NA
Primary Strain
Time (s)
0.25
0.2
0.15
0.1
0.05
0
-0.05
0
1000
2000
3000
4000

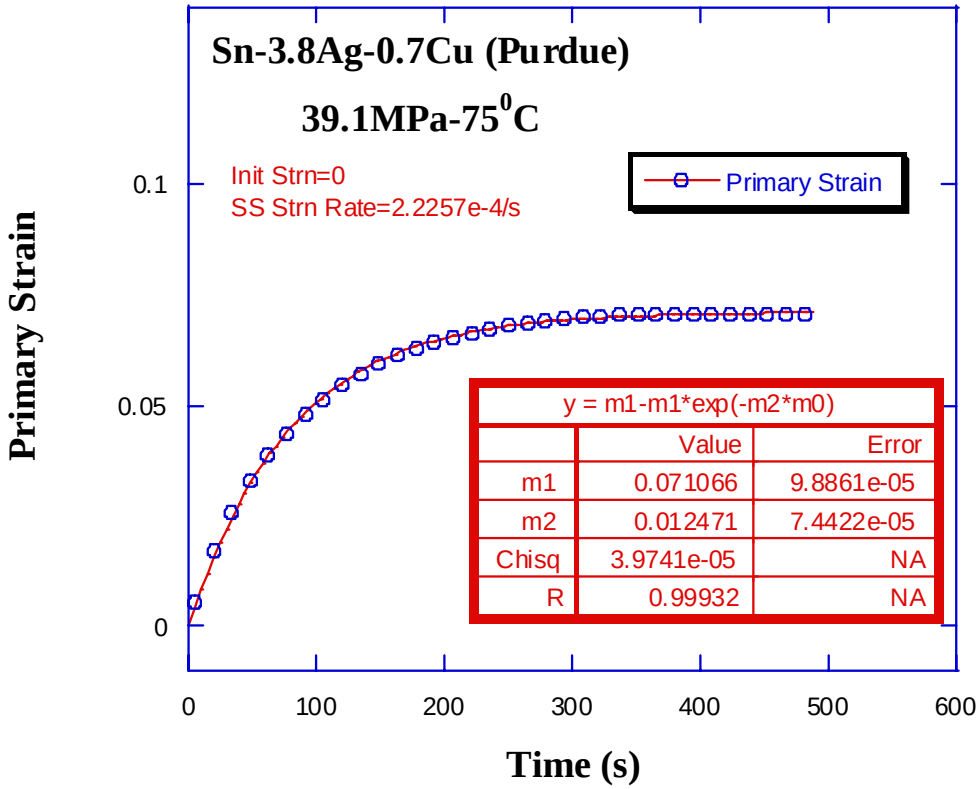
Sn-3.8Ag-0.7Cu (Purdue)
39.1MPa-75^{0}C
Init Strn=0
SS Strn Rate=2.2257e-4/s
Primary Strain
y = m1-m1*exp(-m2*m0)
Value Error
m1 0.071066 9.8861e-05
m2 0.012471 7.4422e-05
Chisq 3.9741e-05 NA
R 0.99932 NA
Primary Strain
Time (s)
0.1
0.05
0
0
100
200
300
400
500
600

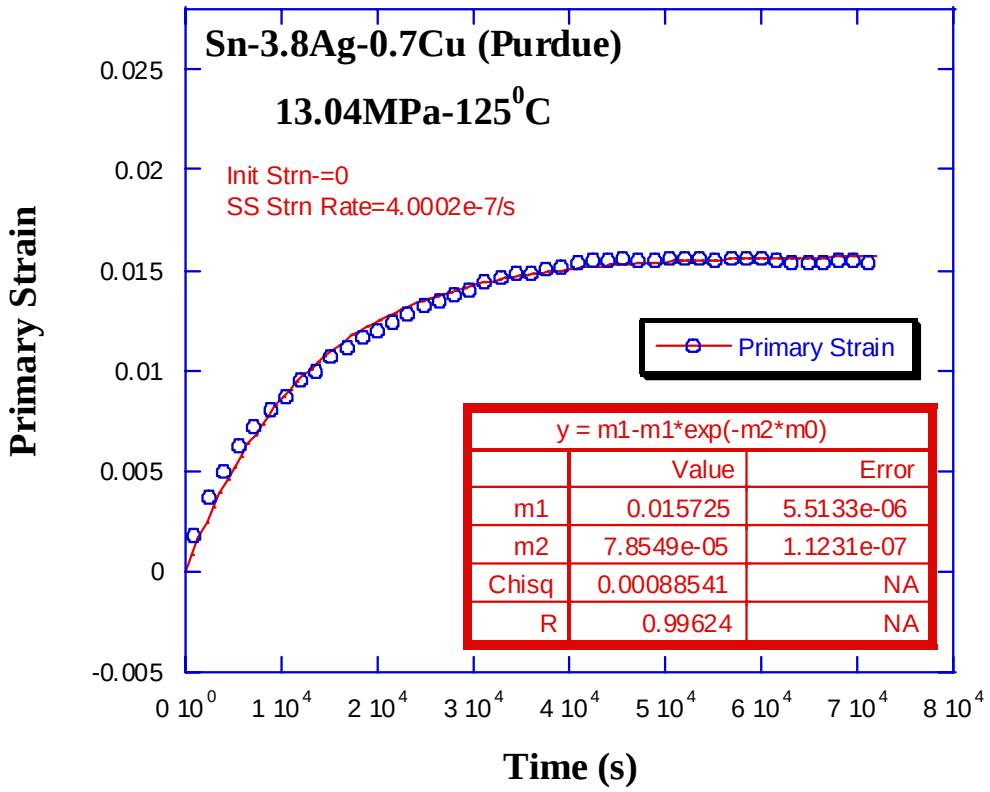
Sn-3.8Ag-0.7Cu (Purdue)
13.04MPa-125^{0}C
Init Strn-=0
SS Strn Rate=4.0002e-7/s
Primary Strain
y = m1-m1*exp(-m2*m0)
Value Error
m1 0.015725 5.5133e-06
m2 7.8549e-05 1.1231e-07
Chisq 0.00088541 NA
R 0.99624 NA
Primary Strain
Time (s)

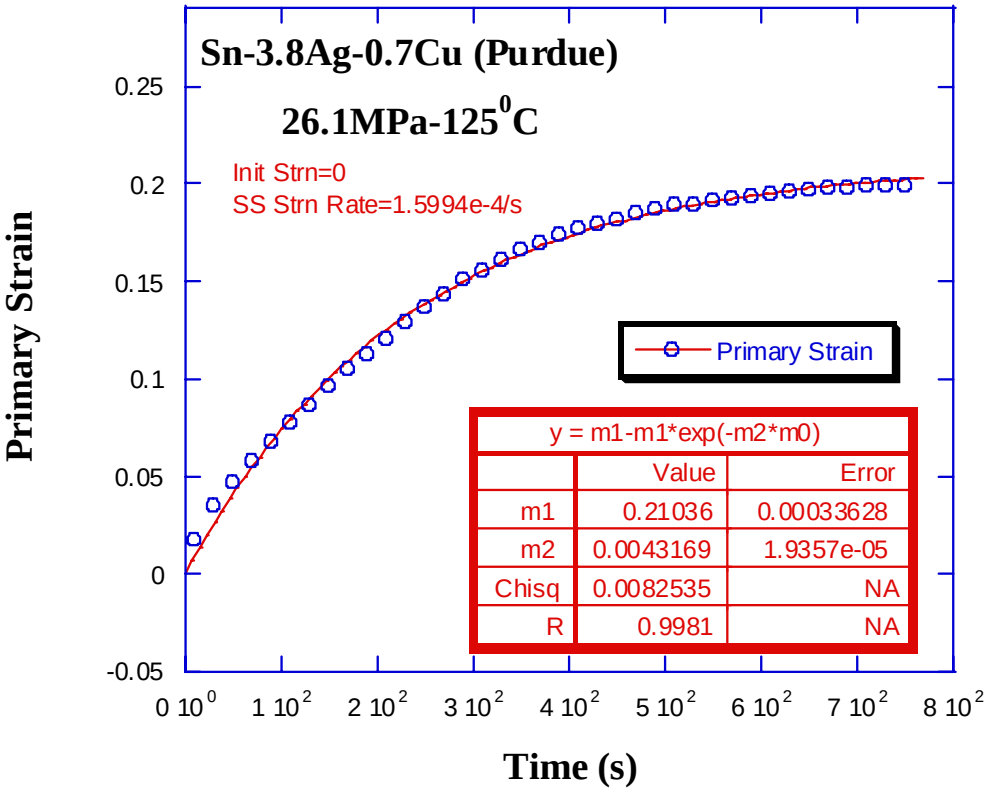
Sn-3.8Ag-0.7Cu (Purdue)
26.1MPa-125^{0}C
Init Strn=0
SS Strn Rate=1.5994e-4/s
Primary Strain
y = m1-m1*exp(-m2*m0)
Value Error
m1 0.21036 0.00033628
m2 0.0043169 1.9357e-05
Chisq 0.0082535 NA
R 0.9981 NA
Primary Strain
Time (s)

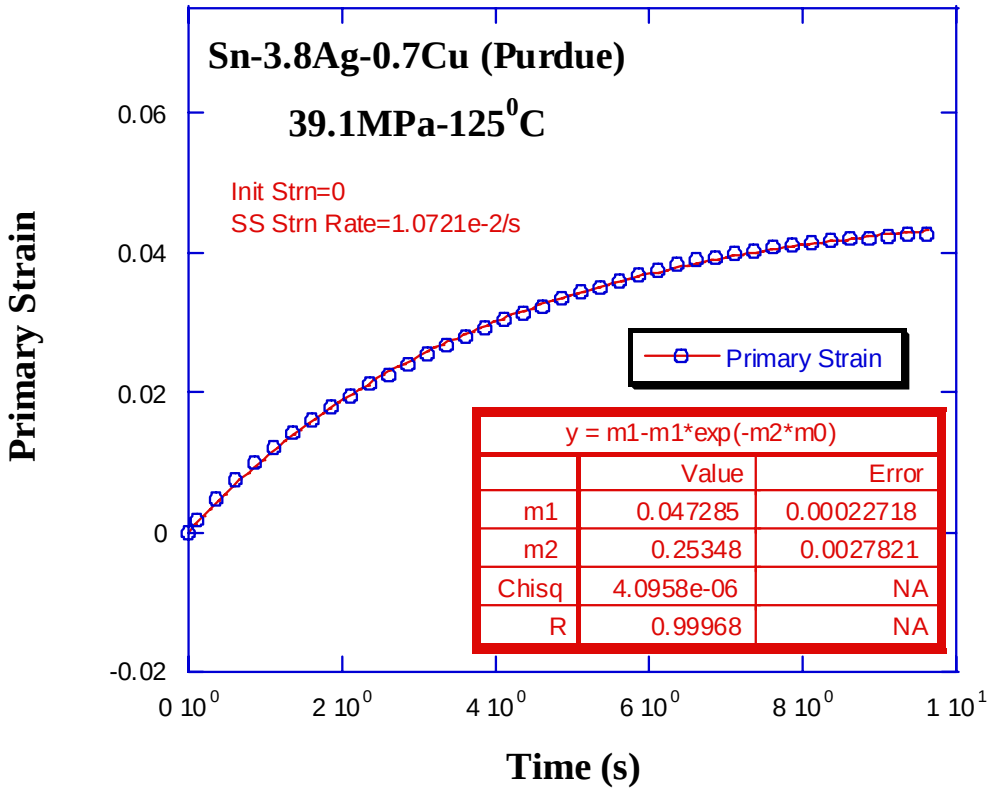
Sn-3.8Ag-0.7Cu (Purdue)
39.1MPa-125^{0}C
Init Strn=0
SS Strn Rate=1.0721e-2/s
Primary Strain
Primary Strain
Time (s)
0.06
0.04
0.02
0
-0.02
0 10^0
2 10^0
4 10^0
6 10^0
8 10^0
1 10^1
y = m1-m1*exp(-m2*m0)
Value
Error
m1
0.047285
0.00022718
m2
0.25348
0.0027821
Chisq
4.0958e-06
NA
R
0.99968
NA

THIS PAGE INTENTIONALLY LEFT BLANK

LIST OF REFERENCES

[1] D.R. FREAR, S.N. BURCHETT, H.S MORGAN, J.H. LAU, "The Mechanics of Solder Alloy Interconnects," Van Nostrand Reinhold, 1994

[2] J. LAU, D. RICE,"Solder Joint Fatigue in Surface Mount Technology: State of the Art," Solid State Technology, pp. 91-104, October 2005.

[3] ZHIGANG CHEN, YAOWU SHI, ZHIDONG XIA, "Constitutive Relations on Creep for Sn-Ag-Cu-RE Lead-Free Solder Joints," Journal of Electronic Materials, Vol. 33, No 9, 2004.

[4] ONOFRIO ANASTASIO, "An Approach for impression Creep of Lead-Free Microelectronic Solder," Center for Materials Science and Engineering, Department of Mechanical and Astronautical Engineering, Naval Postgraduate School, 2002.

[5] ROLANDO REUSE, "Thermomechanical Behavior of Monolithic Sn-Ag-Cu Solder and Copper Fiber Reinforced Solders," Center for Materials Science and Engineering, Department of Mechanical and Astronautical Engineering, Naval Postgraduate School, 2005.

[6] COOKSON ELECTRONICS ASSEMBLY MATERIALS, "Technical Specification for SAC-387."

[7] D.PAN, S. JADHAV, R. MAHAJAN, I. DUTTA, "Microstructural Effects on the Creep Behavior of Sn-4Ag-0.5Cu Microelectronic Solder Balls," submitted to Materials Science & Eng A, 2007

[8] X. LONG, I. DUTTA, V. SARIHAN, D.R. FREAR, "Deformation behavior of Sn-3.8Ag-0.7Cu at intermediate Strain Rates: Effect of Microstructure and Test Conditions," submitted to Journal Electronics Materials, April 2007.

[9] M.L. HUANG, C.M.L. WU, L. WANG, "Creep Resistance of Tin-Based Lead-Free Solder Alloys," Journal of Electronic Materials, November 2005, 11, p. 1371.

[10] S. CHOI, J.G. LEE, F. GUO, T.R. BIELER, K.N. SUBRAMANIAN, J. P. LUCAS, “Creep Properties of Ag-Sn Solder Joints containing Intermetallics Particles,” JOM, June 2001; 53, 6, p. 22.

[11] I. DUTTA, D. PAN, R.A. MARKS, S.G. JADHAV, “Effect of thermo-mechanically induced Microstructural coarsening on the evolution of creep response of Sn-Ag based microelectronics solders,” Materials Science and Engineering A 410-411, 2005, 48-52.

[12] I. DUTTA, “A constitutive model for Creep of Lead-Free Solders undergoing Strain-Enhanced Microstructural Coarsening: A First Report,” Journal of Electronic Materials, Vol. 32, 4, 2003.

[13] F. GUO, S. CHOI, J.P. LUCAS, K.N. SUBRAMANIAN, “Microstructural Characterization of reflowed and isothermally-aged Cu and Ag particulate reinforced Sn-3.5Ag composite solders,” Soldering & Surface Mount Technology, Bradford 2001, Vol. 13, Iss. 1, p. 7.

[14] F. GUO, S. CHOI, J.P. LUCAS, K.N. SUBRAMANIAN, “Effects of Reflow on wettability, Microstructure and Mechanical Properties in Lead-free Solders,” Journal of Electronic Materials, Vol. 29, No 10, 2000.

[15] S.K. Kang, P.A. Lauro, D-Y. Shih, D.W. Henderson, K.J. Puttlitz, “Microstructure and Mechanical properties of Lead-Free solders and solders joints used in microelectronic applications,” IBM Journal of Research and Development, July-September 2005; 49, 4/5; ABI/INFORM Global p. 607.

[16] P.L. Hacke, A.F. Sprecher, H. Conrad, “Microstructure coarsening during Thermo-Mechanical Fatigue of Pb-Sn-Solder Joints,” Journal of Electronic Materials; July 1997; 26,7, p. 774.

[17] A.R. Fix, G.A. Lopez, I. Brauer, W. Nuchter, E.J. Mittemeijer, “Microstructural Development of Sn-Ag-Cu Solder Joints,” Journal of Electronics Materials; February 2005; 34,2 p.137.

[18] K.N. Subramanian, T.R. Bieler, J.P. Lucas, “Microstructural Engineering of Solders,” Journal of Electronic Materials; November 1999; 28, 11, p 1176.

[19] J. Sigelko, S. Choi, K.N. Subramanian, J.P. Lucas, T.R. Bieler, “Effect of Cooling on Microstructure and Mechanical Properties of Eutectic Sn-Ag Solder Joints with and without intentionally incorporated Cu_6Sn_5 reinforcements,” Journal of Electronics Materials, Vol. 28, 11, 1999.

[20] D. Lewis, S. Allen, M. Notis, A. Scotch, “Determination of the Eutectic Structure in the Ag-Cu-Sn system,” Journal of Electronic Materials; Vol. 31, 2, 2002.

[21] K.W. Moon, W.J. Boettinger, “Accurately Determining Eutectic Compositions: The Sn-Ag-cu Ternary Eutectic,” JOM; April 2004; 56, 4, p. 22.

[22] M.L. Huang, C.M.L. Wu, L. Wang, “Creep Resistance of Tin-based Lead-Free Solder Alloys,” Journal of Electronic Materials; November 2005; 34, 11, p 1373.

[23] F. Ochoa, J.J. Williams, N. Chawla, “Effects of cooling Rate in Microstructure and Tensile Behavior of a Sn-3.5%Ag Solder,” Journal of Electronic Materials; December 2003; 32, 12, p. 1414.

[24] V. Kumar, Z.Z. Fang, J. Liang, N. Dariavach, “Microstructural Analysis of Free-Lead Solder Alloys,” Metallurgical and Materials Transactions; August 2006; 37A, 8, p. 2505.

[25] C.M.L. Wu, M.L. Huang, “Creep Behavior of Eutectic Sn-Cu Lead-Free Solder Alloy,” Journal of Electronic Materials; May 2002; 31, 5, p. 442.

[26] M.A. Rist, W.J. Plumbridge, S. Cooper, “Creep Constitutive Behavior of Sn-3.8Ag-o.7Cu Solder Using an Internal Stress Approach,” Journal of Electronic Materials; May 2006; 35, 5, p. 1050.

[27] M. Kerr, N. Chawla, “Creep Deformation behavior of Sn-3.5Ag Solder/Cu Couple at small length scale,” Acta Materialia; 2004; 52, pp. 4527-4535.

[28] R. Hetzberg, “Deformation and Fracture Mechanism of Engineering Materials,” Wiley, Fourth Edition, Chapter 4.

[29] C.H. Raeder, G.D. Schmeelk, D. Mitlin, T. Barbieri, W. Yang, L.F. Felto, R.W. Messler, D.B. Knorr, D. Lee, “Isothermal Creep of Eutectic Sn-Bi and Sn-Ag Solder and Solder Joints,” IEEE/CPMT Int’l Electronics Manufacturing Technology Symposium; 1994.

[30] S-Y. Hwang, J-W. Lee, Z-H. Lee, “Microstructure of a Lead-free Composite Solder Produced by an In-Situ Process,” Journal of Electronics Materials; 2002; 31, 11, p. 1304.

[31] F. Guo, J. Lee, K.N. Subramanian, “Creep Behavior of Composite Lead-Free Electronic Solder Joints,” Soldering & Surface Mount Technology; 2003; 15, 1, p. 39.

[32] J. Cadek, “Creep in Metallic Materials,” Elsevier 1988.

[33] R.W. Evans, B. Wilshire, “Creep of Metals and Alloys,” The institute of Metals, October 1985.

[34] A. Zribi, R. Kinyanjui, P. Borgensen, L. Zavalij, E.J. Cotts, “Aspects of the Structural evolution of Lead-Free Solder Joints,” Journal of Electronic Materials; Junee 2002; 54, 6, p. 38.

[35] C.E. Ho, R.Y. Tsai, Y.L. Lin, C.R. Kao, “Effects of Cu concentration on the reactions between Sn-Ag-Cu solders and Ni,” journal of Electronic Materials; June 2002; 31; 6, p.584.

INITIAL DISTRIBUTION LIST

1. Defense Technical Information Center
   Ft. Belvoir, Virginia

2. Dudley Knox Library
   Naval Postgraduate School
   Monterey, California

3. Professor Indranath Dutta
   Mechanical and Astronautical Engineering
   Naval Postgraduate School
   Monterey, California